

1 **rDNA nascent transcripts promote a unique spatial organization during**
2 **mouse early development**

3
4 Martine Chebrout^{1,2,#}, Maimouna Coura Kone^{1,2,3,#}, Habib U. Jan^{1,2,4}, Marie Cournut^{1,2},
5 Martine Letheule^{1,2}, Renaud Fleurot^{1,2,5}, Tiphaine Aguirre-Lavin^{1,2,6}, Nathalie Peynot^{1,2,7},
6 Alice Jouneau^{1,2}, Nathalie Beaujean^{1,2,8} and Amélie Bonnet-Garnier^{1,2*}

7 1) Université Paris-Saclay, UVSQ, INRAE, BREED, 78350, Jouy-en-Josas, France
8 2) Ecole Nationale Vétérinaire d'Alfort, BREED, 94700, Maisons-Alfort, France
9 3) Current address: Laboratoire Biologie et Santé, Equipe Endocrinologie et Biologie de la
10 Reproduction animale Université Félix Houphouët - Boigny / BP V34, Abidjan 01
11 mounakon5@gmail.com

12 4) Current address: Molecular Biology, Department of Pathology, Medical Teaching
13 Institution, Lady Reading Hospital (LRH-MTI) Peshawar Pakistan. <https://orcid.org/0000-0001-9085-7398>, habib.jan@lrh.edu.pk,

15 5) Current address: CNRS, IFCE, INRAE, Université de Tours, PRC, 37380, Nouzilly,
16 France

17 6) Current address: INRAE, PAO, 37380, Nouzilly, France

18 7) Current address: Université Paris Saclay, INRAE, AgroParisTech, GABI, 78350 Jouy-en-
19 Josas, France

20 8) Current address: Univ Lyon, Université Claude Bernard Lyon 1, Inserm, INRA, Stem Cell
21 and Brain Research Institute U1208, USC1361, 69500 Bron, France

22

23 **Short running title:** rDNA spatial organization in mouse embryos

24 # The two authors have an equal contribution.

25 ***Corresponding author:** Amélie Bonnet-Garnier

26 Tel.: +33 1 34 65 23 79;

27 Fax: +33 1 34 65 29 09;

28 email: amelie.bonnet-garnier@inrae.fr

29 **Key words:** mouse, embryos, 3D-FISH, Pol I inhibition, repeated sequences

30

31 **Abstract**

32 During the first cell cycles of the early development, the chromatin of the embryo is highly
33 reprogrammed alongside that embryonic genome starts its own transcription. The spatial
34 organization of the genome is a major process that contributes to regulating gene transcription
35 in time and space, however, it is poorly studied in the context of early embryos. To study the
36 cause and effect link between transcription and spatial organization in embryos, we focused
37 on the ribosomal genes, that are first silent and begin to transcribe during the 2-cell stage in
38 mouse. We demonstrated that ribosomal sequences are spatially organized in a very peculiar
39 manner from the 2-cell to the 16-cell stage with transcription and processing of ribosomal
40 RNAs excluding mutually. Using drugs inhibiting the RNA polymerase I, we show that this
41 organization, totally different from somatic cells, depends on an active transcription of
42 ribosomal genes and induces a unique chromatin environment that favors major satellite
43 sequences transcription after the 4-cell stage.

44

45 **Abbreviations**

- 46 5'ETS: 5' externally transcribed spacer
47 ActD: Actinomycin D
48 EGA: Embryonic Genome Activation
49 hphCG: hours post-injection of human Chorionic Gonadotrophin
50 H3K9ac: Histone 3 acetylated in lysine 9
51 H3K4me3: Histone 3 tri-methylated in lysine 4
52 ITS1: internal transcribed spacer 1
53 ITS2: internal transcribed spacer 2
54 Major sat: mouse major satellite sequences
55 NPB: Nucleolar Precursor Body
56 Nopp140: Nucleolar phosphoprotein of 140 kD
57 mPN: maternal pronucleus
58 pPN: paternal pronucleus
59 PVP: Poly Vinyl Pyrrolidone
60 RT-qPCR: Real-Time quantitative PCR
61 RNA polymerase I: RNA pol I
62 rDNA: ribosomal DNA genes/sequences
63 rRNA: ribosomal RNA
64 UBF: Upstream Binding Factor
65

66 **Introduction**

67

68 In eukaryotes, the spatial organization of the genome within the interphasic nuclei is
69 not random. DNA fluorescent in situ hybridization (DNA-FISH) experiments have
70 demonstrated that chromosomes occupy a specific nuclear position called territories ((Cremer
71 and Cremer, 2001) and that transcriptional activity may dictated gene positioning reviewed in
72 (Meaburn, 2016). The three-dimension (3D) organization of chromatin acts as a key
73 component of the cell identity and can be correlated with highly differentiated cell types
74 (Solovei et al., 2009). However, the relationships between genome organization and gene
75 transcription is still a matter of debate, albeit after extensive studies reviewed in (van Steensel
76 and Furlong, 2019). For a decade, chromosome conformation capture techniques (3C, 4C and
77 Hi-C) offer the possibility to study whole-genome organization, long-distance interaction, and
78 loops between genomic regions or loci (reviewed in (Bonev and Cavalli, 2016). But
79 depending on the biological model, DNA-FISH and microscopy are still relevant and at least
80 complementary to these approaches (Szabo et al., 2020) allowing single-cell analysis in intact
81 nuclei (Gelali et al., 2019) and localization of repeated sequences such as pericentromeric and
82 centromeric regions of ribosomal DNA (rDNA) genes (Maiser et al., 2020; Mayer et al.,
83 2005).

84 As for mammalian embryos, 3D-FISH of pericentromeric regions (comprising minor
85 and major satellite sequences, (Guenatri et al., 2004)) has been extensively used to
86 demonstrate that these regions undergo large-scale reorganization during the early embryonic
87 development period (reviewed in (Jansz and Torres-Padilla, 2019)). We and others have shown
88 that dramatic changes occur throughout the two first cell cycles of mouse preimplantation
89 development concomitantly with the onset of embryonic transcription (also called embryonic
90 genome activation (EGA)) (Aguirre-Lavin et al., 2012; Bonnet-Garnier et al., 2018; Probst et

91 al., 2007). This spatial reorganization of heterochromatin was shown to be required for further
92 development (Casanova et al., 2013; Probst et al., 2010), highlighting its importance.
93 Remarkably, in 1-cell and early 2-cell mouse embryos, major (and minor) satellite sequences
94 surround dense, spherical structures called nucleolar precursor bodies (NPBs -(Fléchon and
95 Kopecny, 1998)). While, the NPBs were first described as a seed for embryonic nucleolus to
96 settle (Zatsepina et al., 2003), it is now believed that they serve rather as a structural platform
97 anchoring heterochromatin and allowing its remodeling (Fulka and Langerova, 2019). At the
98 time of EGA, satellite sequences indeed progressively disconnect from these NPBs while
99 forming round shape clusters as found in somatic cells and called chromocenters (Aguirre-
100 Lavin et al., 2012). Recently, (Hamdane et al., 2016) have shown that embryos lacking the
101 nucleolar protein UBF also lack NPBs and display an abnormal distribution of
102 heterochromatin. However, the precise relationship between these sequences and the NPBs
103 remains unclear.

104 The inner organization of NPBs has been thoroughly investigated (Baran et al., 1995;
105 Baran et al., 2001; Koné et al., 2016) by immunofluorescent staining of nucleolar proteins
106 such as Upstream Binding Transcription Factor (UBTF), Fibrillarin, B23/Nucleophosmin 1
107 (NPM1), and Nopp140/NOLC1 (Nucleolar and Coiled-body phosphoprotein 1) showing
108 dynamic redistribution of the different nucleolar compartments (mainly the dense fibrillar
109 component, (DFC) and the fibrillar center, (FC)) between the 2-cell and blastocyst stages
110 (time of implantation). The NPBs also structurally support the ribosomal genes (rDNA)
111 (Romanova, 2006). Remarkably, reinitiating of ribosomal transcription (rRNA synthesis) has
112 been shown - by BrUTP incorporation (Zatsepina et al., 2003) - to occur in NPBs at the end of
113 the 2-cell stage, when pericentromeric repeats undergo massive reorganization. It could be
114 that the chromatin state of both rDNA and pericentromeric sequences influence each other as
115 described in Embryonic stem cells (Guetg et al., 2010; Savić et al., 2014). Little is known

116 regarding the spatial organization and expression of rDNA genes in the nuclei of mouse
117 embryos.

118 In the somatic nuclei, the ribosomal genes are transcribed in the nucleolus by the RNA
119 polymerase I (RNA pol I) in a long precursor transcript called 47S pre-rRNA, that will be
120 cleaved by several exonucleases to separate the internal transcribed spacers 1 (ITS1) and 2
121 (ITS2) and the 5' and 3' external transcribed spacers (5'-ETS and 3'-ETS) from the mature
122 ribosomal RNAs (rRNAs): 18S, 5.8S, and 28S (Henras et al., 2015). These rRNAs are
123 associated with ribosomal proteins in pre-ribosomes particles, processed/matured by several
124 proteins, and exported in the cytoplasm to form the small and large ribosome subunits
125 (Mullineux and Lafontaine, 2012). Two proteins: the UBF and the Selective factor 1 (SL1)
126 are required to load the Pol I complex and initiate transcription of the rDNA (Moss et al.,
127 2019). Experimental disruption of the rDNA transcription can be done using either
128 Actinomycin D that intercalates into DNA at the actively transcribed rDNA sites and inhibits
129 pre-rRNA chain elongation (Schöfer et al., 1996) or CX-5461 that specifically inhibits Pol I
130 transcription of rDNA genes by selectively targeting the SL1 transcription factor (Drygin et
131 al., 2011). Studies have shown that these inhibitors are able to affect nucleolar structure
132 organization, reviewed in (Grummt, 2013; Mangan et al., 2017; Potapova and Gerton, 2019).

133 With the use of these specific inhibitors, we will address the organization of rDNA in
134 time and space with regards to major satellite sequences during early embryonic development
135 by 3D-FISH. We will also analyze expression of the various rRNA transcripts to decipher the
136 causal relationship between the spatial organization and the expression changes of these
137 sequences.

138

139 **Results**

140 ***Ribosomal genes (rDNA) 3D organization is linked to their transcription status during***
141 ***preimplantation development***

142 To determine the spatial distribution of rDNA repeats concomitantly with major
143 satellite sequences in mouse early embryo nuclei, 3D-DNA-FISH was performed using
144 probes specific to mouse rDNA repeats (Akhmanova et al., 2000; van de Nobelen et al., 2010)
145 and major satellite sequences (Aguirre-Lavin et al., 2012), respectively. Preservation of the
146 3D structure of the whole embryos allowed us to do in-depth localization of these sequences
147 from the 1-cell to the blastocyst stage (Fig. 1A and 1C, Fig. S1A and S1B).

148 As expected during the 1-cell stage, major satellite sequences progressively formed a
149 ring that surrounded NPBs (Fig. S1A, (Aguirre-Lavin et al., 2012). rDNA signals correspond
150 to large foci (Fig. 1A and Fig. S1A) and are always associated with major satellite sequences
151 irrespective of the origin of the pronucleus (mPN or pPN). At the 2-cell stage, rDNA FISH
152 signals have a small spots shape close to large signal of major satellite sequences and can be
153 divided into two categories: (i) some of them are not associated with NPBs (green arrows in
154 Fig. 1A) and (ii) some of them are embedded within the ring of major satellite sequences
155 surrounding the NPBs (black and white arrows in Fig. S1A). Interestingly, at the late 1-cell
156 and early 2-cell (2-cell E) stages, these rDNA signals are localized at the outer edge of the
157 NPBs (Fig. 1A) as demonstrated by plot profiles of fluorescence intensities for DAPI, major
158 sequences, and rDNA signals across NPBs (mPN, pPN and 2 -cell E in Fig. 1B). At the end of
159 the 2-cell stage (2-cell L) concomitantly with the embryonic genome activation (Zatsepina et
160 al., 2003), rDNA FISH signals change in shape and localization: forming pearl necklace
161 structures (arrowhead in Fig. 1A) juxtaposed to major satellites and extending inside the
162 NPBs (green pick inside NPB2, plot profile at 2-cell L in Fig. 1B).

163 From the early 4-cell to the late 8-cell stage, rDNA signals that were mostly located at
164 the surface of NPBs, lose the pearl necklace shape to form a dispersed cloud of smaller dots,
165 being less and less associated with major satellite sequences (Fig. 1C) and more and more
166 inside the NPBs (as shown by plot profiles drawn across NPBs, Fig. 1D). Finally, the 3D
167 rDNA organization changes one last time, between the 16-cell and the Morula stage: the FISH
168 signals fill the NPBs (16-cell E, 75hphCG in Fig. S1B) and acquire a nucleolus-like structure
169 (Morula) like in differentiated cells (Junera et al., 1995), with no differences between inner
170 cell mass (ICM) and trophectoderm cells (TE) at the Blastocyst stage (Fig. S1B).

171 Quantification of the number of NPBs per stage revealed that it decreased from the
172 late 2-cell to the 16-cell stage (black line in Fig. S1C) and that the remaining NPBs at the 16-
173 cell stage are mostly those associated with the rDNA signal (dark blue bars in Fig. S1C). We
174 then analyzed how rDNA organization evolves and defined four types of NPBs (Fig. 2A,
175 upper panel): T1 corresponding to NPBs with a small number of round-shape rDNA spots; T2
176 corresponding to NPBs with larger spots distributed like a pearl necklace, T3 corresponding
177 to NPBs surrounded by a thin cloud of rDNA signals and T4 corresponding to NBPS with a
178 larger cloud of rDNA signals. Analysis of 350 nuclei from 4-cell to 16-cell stages embryos
179 (Fig. 2A lower panel) shows that T1 and T2 NPBs are predominant at the 4-cell stage and
180 decrease significantly up to the late 8-cell stage ($p\text{-value} < 0.005$). On the other hand, T3
181 NPBs are mostly observed in late 4-cell and early 8-cell stages and T4 NPBs number
182 increases significantly from 8-cell to 16-cell stage ($p\text{-value} < 0.005$, Mann-Whitney U test).

183 To complete our analysis of rDNA 3D-organization, Imaris software (version 9.6,
184 Oxford Instruments) was used to measure the volume of rDNA FISH signals in whole
185 embryos from the 2-cell to 16-cell stage (Fig. S1D) and the corresponding nuclear volume
186 (stained with DAPI, Fig. S1E). To correct for the potential variation of the nuclear volumes
187 (Fig. S1E), the total rDNA volume in a nucleus was divided by the volume of this nucleus

188 (Fig. 2B). While we did not observe variations at the 2-cell stage, earlier stages have always
189 significantly lower normalized mean volumes than later ones at 4 and 8-cell stages (Fig 2B,
190 S2D) potentially linked with the cell cycle since the chromatin is condensed into
191 chromosomes during mitosis. The late 4-cell, early, and late 8-cell stage displayed larger
192 rDNA volumes than earlier stages, suggesting an important decondensation of the rDNA
193 sequences as visualized on DNA-FISH images (Fig. 1B, lower panel). Remarkably, such
194 decondensation is confirmed by calculating the mean sphericity of rDNA spots (in a given
195 nucleus) at each stage (Fig. 2C). Indeed, 4-cell and 8-cell stage embryos have significantly
196 lower sphericity mean values (from 0.77 to 0.82, p-value <0.005) when compared to those of
197 2-cell and 16-cell stage embryos (0.88 and 0.85), respectively. With regards to these
198 parameters (rDNA volume and sphericity), the 16-cell stage has to be considered apart as the
199 structure of the signal changes dramatically at this stage when compared to previous stages
200 and because nuclei become asynchronous, and early vs. late stage cannot be distinguished
201 anymore.

202 Altogether, our results show that rRNA sequences change in shape and distribution
203 twice during early development: first between the early and the late 2-cell stage, when rDNA
204 becomes transcriptionally active, and, secondly, between the late 8-cell stage and the 16-cell
205 stage on the commencement of cell differentiation.

206

207 ***rRNA transcription during early development: a two-step dynamic***

208 To investigate the link between 3D organization of rRNA genes and their
209 transcriptional status, localization of probes specific to the classical rRNA (18S and 28S) and
210 to several pre-rRNA regions that are not retained after complete rRNA processing (5'ETS,
211 ITS1 and ITS2, detailed in Materials and Methods section and Table S1) were studied using
212 RNA-FISH on 3D-preserved embryos (Fig. 3A and 3B).

213 No RNA-FISH signal were detected in the nucleus of 1-cell (data not shown) and early
214 2-cell stages (36hphCG, Fig 3A, and Fig S2A and B) irrespective of the probe used. At the
215 late 2-cell stage, the 5'ETS signal (corresponding to the nascent transcripts) is located in
216 DAPI-free regions inside the nuclei (arrowhead in Fig 3A, 2-cell embryo at 45hphCG) and at
217 the periphery of bigger NPBs (arrow in Fig 3A). At the 4-cell and 8-cell stages, its
218 localization shifts from the periphery to the inner part of the NPBs. Finally, at the 16-cell
219 stage (75hphCG, Fig 3A), the 5'ETS signal fills the NPBs (Fig 3A - lower panel). As for the
220 5'ETS probe, the RNA-FISH signal of ITS1 and ITS2 tend to gain space inside the NPBs
221 during progression through early embryonic development (Fig S2 A and B). At the 16-cell
222 stage, ITS2 and 28S as well as ITS1 and 18S are completely intermingled (Fig S2A and B).

223 To complete RNA-FISH data with quantitative data, real-time quantitative PCR (RT-
224 qPCR) using specific pre-rRNA primers (Table S2) were performed. The level of nascent
225 rRNA transcripts (assessed with 47S and 5'ETS specific primers), gradually increased from
226 late 2-cell to early 8 cell stage and then the curve tends to a plateau (Fig 3C, upper panel).
227 ITS1 and ITS2 specific primers allow us to assess the amount of ‘in-process’ pre-rRNAs: a
228 significant increase was observed from the late 4-cell to the 8-cell stage (Fig 3C, lower panel).

229 Finally, to gain insight into a putative correlation between epigenetic marks and
230 transcription of rDNA, we have determined using an immuno-RNA-FISH approach, the
231 distribution of H3K9ac and H3K4me3 together with their co-localization with nascent
232 transcripts (5'ETS probes). These two histone post-translational modifications (PTMs) are
233 canonically associated with actively transcribed genes (Allis and Jenuwein, 2016). From the
234 2-cell to the 8-cell stages, we observed that some H3K9ac bright foci (green arrows in Fig
235 3D) are localized close to 5'ETS RNA-FISH signals (white arrows in Fig 3D). Notably,
236 H3K9ac foci are found at the periphery of 5'ETS signal at 2-cell and 4-cell stages and then
237 dispersed in the 5'ETS cloud inside the NPBs at the 8-cell stage but do not co-localized with

238 the totality of the nascent transcripts (Fig 3D). The same results are found for H3K4me3
239 (green arrows in Fig S2C).

240 In conclusion, in contrast to the nucleolus in the differentiated cells, rDNA
241 transcription and rRNA maturation processes are separated in time and space in the immature
242 nucleolus of the embryos at early stages. The first part of the early development (from the
243 late-2-cell to the 4-cell stage) is mainly dedicated to the initiation of rDNA transcription as
244 revealed by a large number of nascent transcripts and the presence of H3K9ac and H3K4me3
245 localized close to nascent rRNA. The second part of the early development (8-cell and 16-cell
246 stages) is characterized by the maintenance of the initiation of transcription but an increase in
247 the processing of immature pre-rRNAs.

248

249 ***Inhibition of rRNA transcription and its consequences: elongation is impaired not***
250 ***initiation***

251 To further investigate this temporal separation of initiation of the transcription and
252 processing of rRNA, we used two inhibitors of the RNA Polymerase I (RNA Pol I). Embryos
253 at the 1-cell stage were cultured with either CX-5461 (1 μ M) or Actinomycin D (ActD,
254 7.5ng/ μ L) and fixed 24h (2-cell stage) or 48h later (4-cell stage). We confirmed that both CX-
255 5461-treated and ActD-treated embryos arrested their development at the 4-cell stage (Koné
256 et al., 2016). We then localized the nascent rRNA transcripts by immunoRNA-FISH with
257 5'ETS probe as well as two key nucleolar components, UBF and Nopp140 involved in the
258 initiation of rRNA transcription and processing of the pre-RNA, respectively (Koné et al.,
259 2016). In both the treated groups, 5'ETS signal (green arrows in Fig 4A), Nopp140 (red
260 arrows in Fig 4A), and UBF (white arrows in Fig 4A) immunoRNA-FISH patterns are altered
261 compared to the control-untreated group (Fig 4A). As described in Koné et al (2016), in the
262 control group of UBF and 5'ETS, signals are superposed and surrounded by Nopp140 signal

263 and in CX-5461-treated embryos, Nopp140 and UBF form nucleolar caps, reviewed in (van
264 Sluis and McStay, 2017) with 5'ETS signals still localized around NPBs. On the contrary,
265 after 48h of treatment, ActD-treated embryos show a higher disruption than CX-5461-treated
266 embryos with complete segregation between the UBF-5'ETS and Nopp140 signals, suggesting
267 that nascent transcripts are not processed anymore.

268 To test this hypothesis, the number of nascent pre-rRNAs (using primers for 47S-pre
269 rRNA and the 5'ETS regions) and the number of pre-rRNAs in the process (using primers
270 specific to the ITS1 and the ITS2 regions) were assessed by RT-qPCR (Fig 4B and Fig 4C).
271 There was no significant difference between control and treated-embryos at the 2-cell stage.
272 In the CX-5461 condition, the quantity of 47S, 5'ETS, and ITS1 pre-rRNAs were significantly
273 increased (1.8 fold change) between control and the treated 4-cell embryos (Fig 4B, p value<
274 0.01) although we observed a slight decrease in the RNA-FISH signal compared to control
275 (5'ETS FISH signals in Fig 4A, ITS1 and ITS2 FISH signals in Fig 4D). A putative
276 explanation is that CX-5461-treated embryos compensate a lower number of rDNA loci
277 engaged in transcription by a higher rate of transcription on rDNA that was able to initiate
278 transcription by recruitment of SL1 and UBF. On the contrary, we observed a significant (p-
279 value <0.005) decrease of 5'ETS, ITS1, and ITS2 pre-rRNAs in ActD-treated embryos both
280 by RT-qPCR quantification (Fig 4C) and by RNA-FISH (Fig 4A and 4E). In agreement with
281 the hypothesis that Actinomycin D inhibits RNA Pol I elongation, ITS1 and ITS2 display a
282 stronger reduction (Fig 4E) than 5'ETS (Fig 4A, left panel). CX-5461 has no specific effect on
283 rRNA processing compared to Actinomycin D (in congruance with Mars et al 2020).

284 Altogether, these results demonstrate that RNA Pol I inhibition with Actinomycin D
285 treatment during early embryonic development induces transcriptional arrest at the 4-cell
286 stage and a massive reorganization of nucleolar proteins due to an incomplete transcription
287 and processing of the long 47S pre-rRNA.

288

289 ***RNA Pol I inhibition induces changes on the 3D organization of rDNA***

290 To assess the consequences of RNA Pol I inhibition on rDNA organization and the
291 nearby major satellite sequences, DNA-FISH approach was used (Fig. 1). To compare the
292 organization of rDNA and major satellite sequences between the control and treated embryos,
293 the shape of both DNA signals was visualized and analyzed using 3D reconstruction at the 2-
294 cell and 4-cell stages (Fig.5A and 5B) respectively. At the 2-cell stage, the rDNA signals are
295 compacted and juxtaposed to major satellite signals both in the control and treated embryos
296 (green and black arrows in Fig 5A) but their position in regards to NPBs is different between
297 the control (inside NPBs, Ctrl in Fig 5C) and the treated (outside NPBs, CX-5461 and ActD
298 in Fig 5C) embryos, as shown in plot profiles. At the 4-cell stage, the rDNA signal in the
299 treated embryos is less intense than in the control (green arrows in the upper panel, Fig 5B),
300 its spatial distribution is more compact (clusters seem bigger and in lower number) and in
301 ActD-treated embryos, it forms clusters as in 2-cell stage embryos. Plot profiles drawn across
302 the nuclei show that in the CX-5461, rDNA are still inside the NPBs as in the control
303 condition, but not in the ActD condition where rDNA are outside the NPBs, juxtaposed to
304 major satellite sequences (Fig 5D).

305 To assess and quantify the differences in terms of compaction and shape between the
306 control and the treated embryos, rDNA FISH signals were segmented using Imaris software
307 (as previously in Fig 2B and 2C) to measure the volume and the sphericity of the rDNA signal
308 at 2-cell and 4-cell stages (Fig 6A and 6B). In the controlled condition, the mean volume of
309 the rDNA signal increases from the 2-cell to 4-cell stage, and its shape (measured by the
310 sphericity) becomes less round meaning that rDNA sequences decondensed concomitantly
311 with being actively transcribed. At the 2-cell stage, the shape of the rDNA signal is
312 significantly different between the control and the treated embryos (left panel in Fig 6B, p-

313 value <0.005) suggesting that ribosomal sequences are less round in the treated embryos and
314 putatively less compact. At the 4-cell stage, the mean volume of rDNA signal is significantly
315 (p-value <0.005) different between the control and the treated embryos (Fig 6B, 5.31 +/- 1.63
316 in Ctrl vs 0.85+/-0.48 and 0.93+/- 0.27 in CX-5461 and ActD treated embryos, respectively)
317 meaning that rDNA sequences stay tightly compact and clustered upon RNA Pol I inhibition.

318

319 ***Disruption of 3D organization of rDNA with RNA Pol I inhibition has consequences on the***
320 ***transcription of pericentromeric sequences***

321 By paying attention to the major satellite signals (shape and volume) assisted us in
322 pinpointing that their distribution is modified by the drug treatment. Indeed, after 48h of RNA
323 Pol I inhibition, major satellite DNA-FISH signals show a croissant shape- as in 2-cell
324 embryos (red and black arrows in Fig 5B)- whereas they are normally clustered into
325 chromocenters at the 4-cell stage in controls (black arrowhead in Fig 5B). To confirm this
326 further, the mean volume and the sphericity of the DNA-FISH signals of major satellite
327 sequences were measured using Imaris in the control and the treated embryos (Fig S3A and
328 S3B and Fig 6C and 6D). The mean volume of major satellite sequences FISH signals is
329 significantly lower (p-value <0.005) at the 2-cell stage in the treated embryos compared to the
330 control (right panel, Fig 6C). At the 4cell stage, the volume in the control decreases, while
331 there is no change in the treated embryos (left panel, Fig 6C). Furthermore, the decreased
332 sphericity in the treated embryos compared to the control at the 4-cell stage (right panel, Fig
333 6D) means that the major satellite sequences are less round and compact in the treated
334 embryos. Similarly, the mean sphericity of the 4-cell stage in the treated embryos is not
335 significantly different from that of the 2-cell control embryos.

336 Previous studies highlighted that major satellite sequences are specifically transcribed
337 at the 2-cell stage when their shape is less round (Casanova et al., 2013; Probst et al., 2010),

338 therefore we decided to assess major satellite transcription in the treated vs. control embryos
339 by RNA-FISH and RT-qPCR. No difference in the major satellite RNAs was detected
340 between the control and treated embryos at the 2-cell stage, neither by RNA-FISH nor by RT-
341 qPCR (Fig 7A, B and C) however we detected a significant decrease of transcription in the 4-
342 cell stage ActD-treated embryos (Fig 7B, p< 0.005). On the other hand, a housekeeping gene
343 such as *Hprt* (Fig S3C) does not vary in ActD-treated embryos suggesting a reciprocal
344 influence between rDNA and major satellite transcription. As a matter of fact, after the 2-cell
345 stage burst of transcription, the remaining major satellite RNA-FISH spots were always
346 visualized inside the cloud of 5'ETS FISH signal (green arrows in Fig 7D), at the 4-cell, 8-
347 cell, and 16-cell stages (red arrow in Fig 7D) suggesting that rDNA transcription might
348 induce a chromatin environment that favors transcription of major satellite sequences.

349

350 **Discussion**

351 *Spatial organization of rDNA during early development*

352 In this study, we demonstrated that the spatial positioning of ribosomal genes (rDNA)
353 correlates with their transcription activity. In the context of early embryonic development,
354 ribosomal repeat sequences are first clustered at the surface of NPBs, flanked by ring-shaped
355 major satellite sequences (1-cell and early 2-cell). From the late 2-cell to the 16-cell/morula
356 stage, the sequences then expanded in the inner space of the NPBs until complete filling.
357 During this period, rDNA gradually separated spatially from major satellite sequences
358 although they are physically attached on the same chromosome. The cloudy organization of
359 the active ribosomal sequences we observed fits with the localization of UBF as previously
360 described (Fulka and Langerova, 2014; Hamdane et al., 2016; Koné et al., 2016) and is
361 specific to the early embryonic period. This unique nucleolus organization is very different
362 from the somatic ones (Maiser et al., 2020) that can only be found at the morula and

363 blastocyst stages (Lavrentyeva et al., 2015). Interestingly, this second switch in the nucleolus
364 conformation is associated with a second burst of embryonic genes transcription at the
365 morula-to-blastocyst transition described in transcriptomic data (Hamatani et al., 2004;
366 Hamatani et al., 2006; Wang et al., 2004).

367 In parallel to these drastic changes in the spatial organization of the sequences, we
368 show that rRNA synthesis begins at the mid-2-cell stage, first in the small spherical structures
369 outside the NPBs. Then, nascent rRNAs later appear at the surface of some NPBs as
370 previously described (Koné et al., 2016; Lavrentyeva et al., 2015). Therefore, at very early
371 stages (1-cell and 2-cell stages), NPBs can not be considered as a reservoir for pre-rRNAs
372 waiting to be cleaved confirming previous studies (Lavrentyeva et al., 2015; Shishova et al.,
373 2015a; Shishova et al., 2015b). Interestingly, immuno-RNA-FISH revealed that bright spots
374 of H3K9ac and H3K4me3 are located at the vicinity of 5'ETS signal at the 2-cell stage and
375 that these spots are found inside the 5'ETS cloud at later stages. These results are in
376 agreement with ChIP data obtained on mouse embryonic fibroblast or 3T3 cells (Herdman et
377 al., 2017; Zentner et al., 2014) describing an enrichment of these two epigenetic marks on the
378 spacer promoter (UCE core) at the actively transcribed rDNA repeat (Grummt and Längst,
379 2013; Moss et al., 2019).

380

381 *Inhibition of RNA Pol I and its impact on rRNA processing*

382 To decipher the link between the spatial organization of rDNA and their
383 transcriptional activity, we used two drugs that inhibit RNA Pol I activity in two different
384 mechanisms. CX-5461 is a molecule that inhibits the initiation of transcription by impairing
385 the formation of the pre-initiation complex (PIC) (Drygin et al., 2011) whereas Actinomycin
386 D is a DNA intercalant that inhibits elongation by the RNA polymerases (all of them) in a
387 dose-dependent manner (Perry and Kelley, 1970). Several recent studies (Bruno et al., 2020;

388 Mars et al., 2020; Sanij et al., 2020) discussed the specific targets of CX-5461 (SL1 or
389 Topoisomerase II or RRN3) and its mode of action (G-quadruplex stabilization, DNA
390 damage, impairing of DNA replication fork). Notably, Mars et al., (2020) emphasize that RNA
391 Pol I inhibition by CX-5461 is not reversible and can lead to cell death because of DNA
392 damage. To get rid of these putative side effects of CX-5461, ActD was also used in this
393 study.

394 In the early embryonic context, we observed that CX-5461 disrupts the classical
395 tripartite (i.e. FC, DFC and Granular component (GC) (Boisvert et al., 2007; Pederson, 2011))
396 nucleolus organization (this study & Koné et al 2016). In agreement with (Mars et al., 2020),
397 our study demonstrates that CX-5461 has less impact on the elongation process than
398 Actinomycin D. In the treated embryos, Actinomycin D treatment also inhibits nascent rRNA
399 synthesis but induces a complete stop of the long pre-rRNA production (labeled with ITS1
400 and/or ITS2) which in turn induces both dissociation of transcription initiation (labeled by
401 5'ETS and UBF) and processing of rRNA (labeled with Nopp140). It is worth-mentioning that
402 the treated embryos arrested their development at the 4-cell stage most likely because
403 maternally inherited ribosomes are not renewed as demonstrated in the embryos invalid for
404 UBF (Hamdane et al., 2014; Hamdane et al., 2016).

405

406 *The link between major satellite and rDNA sequences transcription*

407 Lastly, we compared rDNA shape, distribution, and transcriptional activity in time and
408 space with regards to major satellite sequences during early development. Indeed, major
409 satellite sequences are drastically reorganized at the time of EGA (Aguirre-Lavin et al., 2012;
410 Probst et al., 2007) and this reorganization is dependent on major satellite transcripts
411 (Casanova et al., 2013; Probst et al., 2010). On the other hand, localization of major satellite
412 sequences around the NPBs is mandatory at the 1-cell stage as demonstrated by enucleolation

413 experiments (Fulka and Langerova, 2014; Kyogoku et al., 2014; Ogushi and Saitou, 2010;
414 Ogushi et al., 2008) and at the early 2-cell stages (Jachowicz et al., 2013) even if in-depth
415 knowledge of the mechanisms involved are still unknown. Growing pieces of evidence
416 propose that NPBs, rather than acting as a precursor of nucleoli, act as a platform or a Velcro
417 for major satellite sequences (Fulka and Aoki, 2016; Padeken and Heun, 2014) thanks to
418 nucleoplasmin 2 (NPM2, (Burns et al., 2003; Inoue and Aoki, 2010; Kyogoku et al., 2014)).
419 In fact injection of sole NPM2 mRNA rescue developmental failure of enucleolated oocytes
420 (Ogushi et al., 2017). Surprisingly, the absence of NPBs induces the earlier formation of
421 chromocenter-like structures at the zygotic stage (Ogushi et al., 2017) although transcription
422 of major satellite sequences is repressed after the end of the 2-cell stage (Fulka and
423 Langerova, 2014). In this study, we show that inhibition of rDNA transcription induces major
424 satellite sequences to change from a chromocenter-like shape to a ring-like shape without
425 increasing their transcription activity. Surprisingly, Actinomycin D treatment induces a
426 decrease of major satellite transcription while other RNA polymerase II-dependent genes are
427 not affected.

428 rDNA spatial organization is disrupted on the inhibition of RNA Pol I and rRNA
429 sequences aggregate, exhibiting a round shape comparable to earlier inactive stages.
430 Similarly, major satellite sequences exhibit a spatial organization that looks like an early 2-
431 cell stage. This loss of chromatin organization in RNA Pol I inhibited embryos can partially
432 explain the decrease of major satellite sequences transcription. After the 2-cell stage, major
433 satellite transcription is severely repressed and only one or two spots of major satellite RNA
434 can be detected per nucleus by RNA-FISH (Probst et al., 2010). Remarkably, these spots were
435 often found inside the 5'ETS cloud (this study), suggesting transcription of major satellite
436 sequences after the 2-cell stage may require a suitable environment that favor transcription. A
437 putative explanation -among others- is that transcription of major satellite sequences, in 4-cell

438 and 8-cell embryos, need the rDNA peculiar chromatin state (Moss et al., 2019; Potapova and
439 Gerton, 2019): nucleosome-free chromatin with UBF that promotes loops formation
440 (Stefanovsky et al., 2001).

441

442

443 **Material and Methods**

444 **Ethics**

445 Animal care and handling were carried out according to the national rules on ethics and
446 animal welfare in the Animal facility (IERP, INRAE, Infectiology of fishes and rodent
447 facility, doi: 10.15454/1.5572427140471238E12, Jouy-en-Josas, C78-720). This work was
448 approved by the French Ministry of Higher Education, Research and Innovation (n°15-55)
449 and the local ethical committee (INRAE Jouy-en-Josas Center). Departmental veterinary
450 regulatory services have delivered habilitation to work with laboratory animals to ABG
451 (n°78–184) who supervised the work.

452

453 **Collection of mouse embryos and culture**

454 Embryos were collected upon superovulation and mating of C57/CBAF1 mice as previously
455 described (Koné et al., 2016). Zygotes were obtained by dissecting the ampulla of the oviduct
456 24 hours post-injection of human chorionic gonadotropin (hCG) and treated briefly with
457 1mg/ml of hyaluronidase (Sigma) in M2 medium (Sigma) to remove follicular cells. Then, 1-
458 cell (24h phCG) embryos were cultured *in vitro* in M16 medium (Sigma) at 37°C in a
459 humidified atmosphere of 5% CO₂ until they reached the adequate stages to be processed:
460 early 2-cell (36h phCG - 2CE), late 2-cell (48h phCG - 2CL), early 4-cell (54h phCG - 4CE),
461 late 4-cell (58h phCG - 4CL), early 8-cell (60h phCG - 8CE), late 8-cell (72h phCG - 8CL),
462 16-cell (75h phCG), Morula (96h phCG) and Blastocyst (110h phCG).

463

464 **CX-5461 and Actinomycin D treatment**

465 Two different RNA Polymerase I (RNA Pol I) inhibitors were used in this study: CX-5461
466 that impairs the formation of the RNA Polymerase I pre-initiation complex (PIC) by
467 disrupting the recruitment of SL1 (Selective factor 1) with UBF (Upstream bidding factor) to

468 the rDNA promoter (Drygin et al., 2011) and Actinomycin D that intercalates into the DNA
469 and thereby inhibits elongation of all the RNA polymerases activity, although with a higher
470 affinity for RNA Pol I (Bensaude, 2011; Perry and Kelley, 1970). These two drugs induce
471 segregation of the nucleolus components dedicated either to transcription (fibrillar and dense
472 fibrillar components -FC and DFC) or to rRNA processing (granular component, GC). These
473 components can be visualized by fluorescent immuno-detection of the proteins involved in
474 these processes (UBF and Nopp140 respectively, as described in (Koné et al., 2016)).
475 Embryos collected at the 1-cell stage (24hphCG) were cultured in M16 medium containing
476 either 1µM of CX-5461 (Adooq) or 7.5ng/µL of Actinomycin D (Sigma) to inhibit RNA Pol I
477 as described respectively in (Bellier, 1997; Koné et al., 2016). Every 24h, the embryos were
478 transferred into new droplets of medium containing the RNA Pol I inhibitors. The treated
479 embryos were fixed at two-time points: 24h and 48h after exposure to the drug and then
480 processed for immunoRNA-FISH / DNA-FISH or frozen dry in low RNA binding tubes and
481 kept at -80°C for RT-qPCR assays.
482

483 **Probes for DNA and RNA-FISH**

484 rDNA and major satellite FISH probes were prepared as described in (Aguirre-Lavin et al.,
485 2012) and (Bonnet-Garnier et al., 2013). Briefly, cosmid containing the entire transcribed
486 sequences (n°13, detailed in (Akhmanova et al., 2000; van de Nobelen et al., 2010) was used
487 for the ribosomal sequences (kind gift from N. Galjart). The amplified rDNA gene fragments
488 were purified using nucleobond AX 100 columns for Miniprep System (Macherey-Nagel, ref
489 740521.100). The rDNA sequences were then labeled with Digoxigenin-11-dUTP by nick
490 translation according to the manufacturer's protocol (Roche, Ref 11277065910). For the
491 detection of major satellites, a probe prepared by PCR on genomic mouse DNA with the
492 primers 5'-CATATTCCAGGTCTTCAGTGTGC-3' and 5'-CACTTTAGGACGTGAAAT

493 ATGGCG-3' was labeled with Cy3 by random priming according to the kit instruction
494 (Invitrogen Kit, Ref 18095–011).

495 Specific oligo-probes (designed from the complete 45S mouse ribosomal sequences -
496 X82564.1 or adapted from (Le Bouteiller et al., 2013; Shishova and others, 2011; Shishova et
497 al., 2015b) directly labeled with a fluorophore in 3' end (sequences are detailed in Table S1)
498 were purchased from Eurogentec. These probes located (Fig. 2B) on different regions of the
499 47S pre-rRNA (Kent et al., 2008) are named: 5'ETS for the probe specific to the external
500 transcribed spacer (rapidly removed, allowing the detection of early transcription sites, i.e.
501 nascent rRNA transcripts), ITS1: specific for the internal transcribed spacer 1 located between
502 the 18S and the 5.8S regions and ITS2: specific for the internal transcribed spacer 2 located
503 between the 5.8S and the 28S region. ITS1 and ITS2 enable the mapping of the region where
504 rRNA processing occurs. Probes specific for 18S and 28S regions were also used to assess if
505 mature or pre-rRNAs were already accumulated in NPBs before the onset of rDNA
506 transcription. Of note, the 18S and 28S probes signal can be detected in the cytoplasm
507 because they are components of ribosomes.

508

509 **DNA-FISH**

510 For DNA-FISH, DNA probes described above specific to either ribosomal or major satellite
511 sequences were used together on the whole embryos. During all the manipulations, drying
512 was avoided to preserve the 3D of nuclei. This protocol is based on (Miyanari and Torres-
513 Padilla, 2012) with slight modifications. The embryos collected at a specific stage were
514 transferred in a 10-well glass dish warm at 37°C. The embryos were rinsed in M2 medium,
515 submitted briefly (less than 15s) to Tyrode's acid solution (Sigma-Aldrich), washed quickly in
516 an M2 with 10mM phenylmethanesulfonyl fluoride (PMSF, Fluka) solution then in a 0.5%
517 polyvinyl-pyrrolidone (PVP) in PBS with 10mM PMSF solution and finally incubated in a

518 fixation/permeabilization solution (4% paraformaldehyde (PFA), 0.5% Triton X-100, 10mM
519 PMSF, 0.5% PVP in PBS) for 15min at 37°C. The embryos were then washed twice in a
520 PBS/PVP 0.5% solution at RT and let at +4°C (at least overnight) in a humid chamber until
521 fixation of other stages. To remove the zona pellucida (ZP), all the embryos were incubated
522 under a stereomicroscope to monitor the ZP vanishing in a 0.1N HCl (Prolabo) solution for 20
523 to 30s (depending on the stage) at RT and transferred to PBS/PVP 0.5%. The ZP removal was
524 achieved by successive passages through a very fine glass pipette when needed. The embryos
525 were permeabilized in a 0.5% Triton X-100 / 200µg/ml RNase solution for 30 min at 37°C
526 and washed twice in 2X saline-sodium citrate (2XSSC) pH 6.3 for 5 min at 37°C. The
527 embryos were then transferred for 3h at 37°C in a humidified chamber in a 20µl drop of
528 hybridization buffer (50% formamide, SCC 2X, Denhardt 1X, 40 mM NaH₂PO₄, 10%
529 dextran sulfate) containing the DNA-FISH probes mix (14µl of rDNA probe solution at
530 50ng/µl and 1µl of major satellite probe solution at 100 ng/µl completed to 20µl with
531 hybridization buffer). The embryos were denatured at 85°C for 10 min on a heating plate and
532 then let three days for hybridization at 37°C in a humid chamber. After hybridization, the
533 embryos were rinsed twice with 2X SSC / 0.1% Triton X-100 / 0.5% PVP for 10 min at 42°C.
534 Embryos were then incubated in a blocking solution (4X SSC / 2% BSA) for 1h at RT and
535 incubated with a primary antibody diluted in blocking solution (sheep anti-digoxigenin, 1/200,
536 Roche) overnight at +4°C in a dark humidified chamber. The embryos were washed twice in
537 4X SSC / 2% BSA / 0.05% Tween20 before and after incubation with the secondary antibody
538 (mouse anti-sheep Ig coupled to FITC, 1/200, 713-095-147, Jackson ImmunoResearch
539 Laboratories Inc., USA) for 1h at RT. The embryos were washed in 2X SSC / 0.5% PVP and
540 gently mounted to preserve the 3D structure of the nuclei between slides (Menzel Superfrost
541 Plus, Thermo Scientific) and cover-slip with a large amount of Vectashield antifading agent
542 (Abcys) containing 10µg/mL DAPI (Invitrogen).

543

544 **RNA-FISH**

545 For RNA-FISH, the embryos were processed almost as for DNA-FISH with two main
546 differences: 1) the ZP was not removed by HCl treatment; 2) an RNase inhibitor (1µL/mL of
547 RNasin - Promega) was added to all the solutions after the fixation/permeabilization step.
548 Briefly, after fixation/permeabilization, embryos were further permeabilized in 0.5% Triton
549 X100 /0.5% PVP-PBS for 45min at 37°C, washed and transferred for 30min at 50°C in the
550 pre-hybridization mix containing 50% Formamide (Sigma-Aldrich); 0.5µg/µL tRNA (Sigma-
551 Aldrich); 1X hybridization buffer (2X hybridization buffer was prepared beforehand with 20%
552 dextran sulfate, 4X SSC; 1mM EDTA, 40mg/mL BSA, 2mg/mL PVP, 0.1% Triton X100,
553 diluted in pure grade water). In parallel, a solution containing the fluorescent oligonucleotide
554 probes (100ng/µl diluted in 1X hybridization buffer) was denatured 10 min at 85°C and
555 immediately put on ice to avoid renaturation of the DNA. The embryos were then transferred
556 in this hybridization mix and incubated overnight at 42°C. The embryos were washed twice
557 in 2XSSC; 0.5%PVP; 0.1% Triton X100 (diluted with pure grade water) for 10min at 37°C
558 and mounted on slides with coverslips as described in the DNA-FISH section.

559

560 **ImmunoRNA-FISH**

561 Immunofluorescence labeling followed by RNA-FISH was performed as described in Kone et
562 al. (2016) with slight modifications. Briefly, the embryos were fixed as described in the RNA-
563 FISH section before immunostaining. The embryos were then permeabilized in 0.5% Triton
564 X100 / 0.5% PVP-PBS for 30min at 37°C and transferred in 2% BSA-PBS 1h at RT. The
565 embryos were incubated with primary antibody overnight at 4°C, washed thrice in 0.5%PVP-
566 PBS, and then incubated with secondary antibody for 1h and post-fixed in 2% PFA/0.5%
567 PVP-PBS for 10 min at RT. The embryos were then further processed for RNA-FISH as

568 described in the RNA-FISH section. All antibodies were diluted in 2% BSA-PBS. Again,
569 RNase inhibitor (1 μ L/mL of RNasin - Promega) was added to all the solutions after the
570 fixation/permeabilization step.

571

572 **Antibodies**

573 Primary antibodies used: anti-UBF (1/100; mouse polyclonal antibody H00007343-M01;
574 Novus Biologicals), anti-Nopp140 (1/150; rabbit polyclonal antibody, RF12 serum; a gift
575 from U. Thomas Meier, Department of Anatomy and Structural Biology, New York, USA),
576 anti-H3K9ac (1/100, rabbit polyclonal antibody, 39917) and anti-H3K4me3 (1/400, rabbit
577 polyclonal antibody, ab8550, Abcam). Secondary antibodies used: IgG donkey anti-mouse
578 Cy3 (1/200, 715-025-151, Jackson ImmunoResarch) and IgG donkey anti-rabbit Cy5 (1/200,
579 111-175-152, Jackson ImmunoResarch).

580

581 **Confocal microscopy and image analyses**

582 Imaging was performed with a ZEISS LSM 700 confocal laser scanning microscope
583 (MIMA2, INRAE, Microscopy and Imaging Facility for Microbes, Animals and Foods,
584 <https://doi.org/10.15454/1.5572348210007727E12>) equipped with a 63X (1.4 NA) oil
585 immersion objective. Z-stacks were acquired with a frame size of 512 \times 512 or 1024 \times 1024, a
586 pixel depth of 8 bits, and a z-distance of 0.37 μ m between optical sections. Fluorescence
587 wavelengths of 405, 488, 555, and 639 nm were used to excite DAPI, Alexa-488, or FITC,
588 Cy3, and Cy5, respectively.

589 Fluorescent profiles measurement were generated in Fiji (Schindelin et al., 2012; Schindelin
590 et al., 2015; Schneider et al., 2012) and 3D reconstructions using AMIRA 3.1 software
591 (Mercury Computer Systems, Berlin, Germany, (Stalling et al.)

592 Quantitative image analysis was performed manually using Imaris 9.6 software (Oxford
593 Instruments) available at the MIMA2 ISC INRAE. Briefly, in 10 embryos of each stage,
594 nuclei were first segmented using an automatically set threshold (wizard function in Imaris
595 surfaces package). Major satellites and rDNA signals were then segmented in a specified
596 region of interest (ROI defined by the nucleus label) following the same process. For all
597 detected objects, several values (area, volume, sphericity, numbers) were calculated by Imaris
598 and exported for statistical analysis in Microsoft Excel file format. For each analyzed nuclei,
599 the sum of the volume of DNA-FISH signals was calculated to obtain the total volume of
600 rDNA or major satellite DNA-FISH signals in a given nucleus. Then this total volume was
601 normalized by the volume of the given nucleus using this formula: (Vol_tot_{FISH} /
602 Vol_tot_{nucleus})x 100, to circumvent any nucleus size effect when comparing between stages.

603

604 **RT-qPCR**

605 The embryos at each stage were pooled by a batch of 10 and snap-frozen. Total RNA was
606 prepared without purification using the SingleShot Cell Lysis kit (Biorad) that includes
607 DNase treatment. cDNA was prepared directly from the lysates with random hexamers (300
608 ng) (Lifetechnologies, France) following the supplier's protocol (25°C for 5 min, 50°C for 60
609 min and 70°C for 15 min) in the presence of 10 fg of Luciferase RNA (Promega) using the
610 SuperScript III reverse transcription kit (Invitrogen). Negative controls without reverse
611 transcriptase were prepared the same way. RT-qPCR was performed on 0.2 or 0.032 embryo
612 equivalent (as described in Salvaing et al 2016), depending on the genes, using KAPA SYBR
613 FAST (Roche) or SYBR Green (Applied, for Major satellites) master mix on a StepOne Plus
614 cycling machine (Applied). The difference in amplification of positive and negative samples
615 was at least 5 Ct (5 to 9). To avoid biais due to a highly variable amount of transcript from
616 endogenous genes (Hprt1) before the EGA, the results were finally normalized to Luciferase

617 (as described in Bui et al). Primers are listed in Table S2. Three to six biological replicates
618 were used.

619

620 **Statistical analyses**

621 All the statistical analyses and tests were performed using R packages. Several R packages
622 such as ggplot2 and lattice were used in complement to Rcmdr packages to generate graphs.
623 The normality and homogeneity of variances were tested using the 'shapiro.test' and
624 'bartlett.test' R-packages, respectively. As the sample size was small (<30), non-parametrical
625 tests were used. Two by two comparison were done using 'wilcox' packge (Mann-Whitney-
626 Wilcoxon) and comparison of the two consecutive stages were done with 'nparcomp' package
627 (Nonparametric Multiple Comparisons).

628

629 **Supplementary material**

630 Figs. S1–S5 show 3D organization of ribosomal sequences (rDNA) at 1-cell stage, 16-cell and
631 morula to blastocyst stages using DNA-FISH, the number of nucleolar precursor bodies
632 (NPBs), Quantification of the volume of nucleus and rDNA FISH signals using Imaris,
633 Localization by RNA-FISH of several ribosomal RNA (rRNA) from 2-cell to 16-cell stages,
634 Localization of H3K4me3 and nascent transcripts of rRNA by immunoRNA-FISH,
635 Quantification of major satellite sequences volume and sphericity from 2-cell up to 16-cell
636 stage and relative expression of an housekeeping gene (*Hprt*) by RT-qPCR in control and
637 treated embryos.

638 Tables S1–S2 show the list of oligoprobes used for the RNA-FISH and the list of primers
639 used in th RT-qPCR experiments respectively.

640 **Acknowledgements**

641 We would like to thank Prof. Galjart Niels (Nederland), M Cohen-Tanoudji (Pasteur
642 Institute), and Janice Britton Davidian lab (Montpellier) for their kind gifts of rDNA
643 plasmids/cosmids and the RNA-FISH probes. We also thank Claire Boulesteix for her
644 technical assistance and laboratory facilities and Bertrand Bed'hom for his help with Imaris
645 analysis. We thank the ISC MIMA2 (Microscopy and Imaging Facility for Microbes, Animals
646 and Foods, doi: 10.15454/1.5572348210007727E12) and particularly Pierre Adenot for
647 advice in 3D images analyses with ImageJ and Imaris. We acknowledge the staff of the
648 INRAE Infectiology of Fishes and Rodents Facility (IERP-UE907, Jouy-en-Josas Research
649 Center, France) in which animal experiments have been performed. IERP Facility belongs to
650 the National Distributed Research Infrastructure for the Control of Animal and Zoonotic
651 Emerging Infectious Diseases through In Vivo Investigation (EMERG'IN DOI:
652 10.15454/1.5572352821559333E12).

653 This project was funded by the REVIVE Labex (Investissement d'Avenir, ANR-10-LABX-
654 73) and supported by the PHASE Department of the French National Research Institute for
655 Agriculture, Food and Environment (INRAE).

656 The authors declare no competing financial interests.

657

658 **Authors contribution**

659 M. Chebrout set up the RNA-FISH and immunoRNA-FISH experiments, performed majority
660 of the experiments, and analyzed the data. M.C. Koné, M. Cournot and H.U Jan performed
661 and analyzed DNA-FISH experiments. R. Fleurot and T. Aguirre-Lavin set up and performed
662 the DNA-FISH experiments. A. Jouneau and N. Peynot performed and analyzed the RT-
663 qPCR experiments. N. Beaujean secured funding, gave guidance during initial data
664 production and analysis, and made early corrections to the manuscript. A. Bonnet-Garnier
665 supervised, directed, and designed the study, analyzed, and interpreted the data, made the
666 figures, and wrote the article. All the authors reviewed and commented on the manuscript.

667

668 **Ethical approval**

669 All applicable international, national, and/or institutional guidelines for the care and use of
670 animals were followed. This article does not contain any studies with human participants
671 performed by any of the authors.

672

673 **References**

- 674 **Adenot, P. G., Mercier, Y., Renard, J.-P. and Thompson, E. M.** (1997). Differential H4 acetylation of
675 paternal and maternal chromatin precedes DNA replication and differential transcriptional
676 activity in pronuclei of 1-cell mouse embryos. *Development* **124**, 4615–4625.
- 677 **Aguirre-Lavin, T., Adenot, P., Bonnet-Garnier, A., Lehmann, G., Fleurot, R., Boulesteix, C., Debey, P.**
678 **and Beaujean, N.** (2012). 3D-FISH analysis of embryonic nuclei in mouse highlights several
679 abrupt changes of nuclear organization during preimplantation development. *BMC Dev. Biol.*
680 **12**, 30.
- 681 **Akhmanova, A., Verkerk, T., Langeveld, A., Grosveld, F. and Galjart, N.** (2000). Characterisation of
682 transcriptionally active and inactive chromatin domains in neurons. *J. Cell Sci.* **113**, 4463–
683 4474.
- 684 **Allis, C. D. and Jenuwein, T.** (2016). The molecular hallmarks of epigenetic control. *Nat. Rev. Genet.*
- 685 **Baran, V., Veselá, J., Rehák, P., Koppel, J. and Fléchon, J. E.** (1995). Localization of fibrillarin and
686 nucleolin in nucleoli of mouse preimplantation embryos. *Mol Reprod Dev* **40**,
- 687 **Baran, V., Brochard, V., Renard, J. P. and Flechon, J. E.** (2001). Nopp 140 involvement in
688 nucleologenesis of mouse preimplantation embryos. *Mol. Reprod. Dev.* **59**, 277–284.
- 689 **Bellier, S.** (1997). Nuclear translocation and carboxyl-terminal domain phosphorylation of RNA
690 polymerase II delineate the two phases of zygotic gene activation in mammalian embryos.
EMBO J. **16**, 6250–6262.
- 692 **Bensaude, O.** (2011). Inhibiting eukaryotic transcription. Which compound to choose? How to
693 evaluate its activity?: Which compound to choose? How to evaluate its activity? *Transcription*
694 **2**, 103–108.
- 695 **Boisvert, F.-M., van Koningsbruggen, S., Navascués, J. and Lamond, A. I.** (2007). The multifunctional
696 nucleolus. *Nat. Rev. Mol. Cell Biol.* **8**, 574–585.
- 697 **Bonev, B. and Cavalli, G.** (2016). Organization and function of the 3D genome. *Nat. Rev. Genet.* **17**,
698 661–678.
- 699 **Bonnet-Garnier, A., Feuerstein, P., Chebrout, M., Fleurot, R., Jan, H.-U., Debey, P. and Beaujean, N.**
700 (2013). Genome organization and epigenetic marks in mouse germinal vesicle oocytes. *Int. J.*
701 *Dev. Biol.* **56**, 877–887.
- 702 **Bonnet-Garnier, A., Kiêu, K., Aguirre-Lavin, T., Tar, K., Flores, P., Liu, Z., Peynot, N., Chebrout, M.,**
703 **Dinnyés, A., Duranthon, V., et al.** (2018). Three-dimensional analysis of nuclear
704 heterochromatin distribution during early development in the rabbit. *Chromosoma* **127**,
705 387–403.
- 706 **Bruno, P. M., Lu, M., Dennis, K. A., Inam, H., Moore, C. J., Sheehe, J., Elledge, S. J., Hemann, M. T.**
707 **and Pritchard, J. R.** (2020). The primary mechanism of cytotoxicity of the chemotherapeutic
708 agent CX-5461 is topoisomerase II poisoning. *Proc. Natl. Acad. Sci.* **117**, 4053–4060.
- 709 **Bui, L. C., Esvikov, A. V., Khan, D. R., Archilla, C., Peynot, N., Hénaut, A., Le Bourhis, D., Vignon, X.,**
710 **Renard, J. P. and Duranthon, V.** (2009). Retrotransposon expression as a defining event of

- 711 genome reprogramming in fertilized and cloned bovine embryos. *REPRODUCTION* **138**, 289–
712 299.

713 **Burns, K. H., Viveiros, M. M., Ren, Y., Wang, P., DeMayo, F. J., Frail, D. E., Eppig, J. J. and Matzuk,**
714 **M. M.** (2003). Roles of NPM2 in chromatin and nucleolar organization in oocytes and
715 embryos. *Science* **300**, 633–6.

716 **Casanova, M., Pasternak, M., El Marjou, F., Le Baccon, P., Probst, A. V. and Almouzni, G.** (2013).
717 Heterochromatin Reorganization during Early Mouse Development Requires a Single-
718 Stranded Noncoding Transcript. *Cell Rep.* **4**, 1156–1167.

719 **Cremer, T. and Cremer, C.** (2001). Chromosome territories, nuclear architecture and gene regulation
720 in mammalian cells. *Nat Rev Genet* **2**, 292–301.

721 **Drygin, D., Lin, A., Bliesath, J., Ho, C. B., O'Brien, S. E., Proffitt, C., Omori, M., Haddach, M.,**
722 **Schwaebbe, M. K., Siddiqui-Jain, A., et al.** (2011). Targeting RNA Polymerase I with an Oral
723 Small Molecule CX-5461 Inhibits Ribosomal RNA Synthesis and Solid Tumor Growth. *Cancer*
724 *Res.* **71**, 1418–1430.

725 **Fléchon, J.-E. and Kopecny, V.** (1998). The nature of the ‘nucleolus precursor body’ in early
726 preimplantation embryos: a review of fine-structure cytochemical, immunocytochemical and
727 autoradiographic data related to nucleolar function. *Zygote* **6**, 183–191.

728 **Fulka, H. and Aoki, F.** (2016). Nucleolus Precursor Bodies and Ribosome Biogenesis in Early
729 Mammalian Embryos: Old Theories and New Discoveries. *Biol. Reprod.* **94**,

730 **Fulka, H. and Langerova, A.** (2014). The maternal nucleolus plays a key role in centromere satellite
731 maintenance during the oocyte to embryo transition. *Development* **141**, 1694–1704.

732 **Fulka, H. and Langerova, A.** (2019). Nucleoli in embryos: a central structural platform for embryonic
733 chromatin remodeling? *Chromosome Res.* **27**, 129–140.

734 **Gelali, E., Girelli, G., Matsumoto, M., Wernersson, E., Custodio, J., Mota, A., Schweitzer, M., Ferenc,**
735 **K., Li, X., Mirzazadeh, R., et al.** (2019). iFISH is a publicly available resource enabling
736 versatile DNA FISH to study genome architecture. *Nat. Commun.* **10**, 1636.

737 **Grummt, I.** (2013). The nucleolus—guardian of cellular homeostasis and genome integrity.
738 *Chromosoma* **122**, 487–497.

739 **Grummt, I. and Längst, G.** (2013). Epigenetic control of RNA polymerase I transcription in
740 mammalian cells. *Biochim. Biophys. Acta BBA-Gene Regul. Mech.* **1829**, 393–404.

741 **Guenatri, M., Bailly, D., Maison, C. and Almouzni, G.** (2004). Mouse centric and pericentric satellite
742 repeats form distinct functional heterochromatin. *J. Cell Biol.* **166**, 493–505.

743 **Guetg, C., Lienemann, P., Sirri, V., Grummt, I., Hernandez-Verdun, D., Hottiger, M. O., Fussenegger,**
744 **M. and Santoro, R.** (2010). The NoRC complex mediates the heterochromatin formation and
745 stability of silent rRNA genes and centromeric repeats. *EMBO J* **29**,

746 **Hamatani, T., Carter, M. G., Sharov, A. A. and Ko, M. S. H.** (2004). Dynamics of global gene
747 expression changes during mouse preimplantation development. *Dev Cell* **6**,

- 748 **Hamatani, T., Ko, M. S., Yamada, M., Kuji, N., Mizusawa, Y., Shoji, M., Hada, T., Asada, H.,**
749 **Maruyama, T. and Yoshimura, Y.** (2006). Global gene expression profiling of preimplantation
750 embryos. *Hum. Cell* **19**, 98–117.
- 751 **Hamdane, N., Stefanovsky, V. Y., Tremblay, M. G., Németh, A., Paquet, E., Lessard, F., Sanij, E.,**
752 **Hannan, R. and Moss, T.** (2014). Conditional Inactivation of Upstream Binding Factor Reveals
753 Its Epigenetic Functions and the Existence of a Somatic Nucleolar Precursor Body. *PLoS*
754 *Genet.* **10**, e1004505.
- 755 **Hamdane, N., Tremblay, M. G., Dillinger, S., Stefanovsky, V. Y., Németh, A. and Moss, T.** (2016).
756 Disruption of the UBF gene induces aberrant somatic nucleolar bodies and disrupts embryo
757 nucleolar precursor bodies. *Gene*.
- 758 **Henras, A. K., Plisson-Chastang, C., O'Donohue, M.-F., Chakraborty, A. and Gleizes, P.-E.** (2015). An
759 overview of pre-ribosomal RNA processing in eukaryotes. *WIREs RNA* **6**, 225–242.
- 760 **Herdman, C., Mars, J.-C., Stefanovsky, V. Y., Tremblay, M. G., Sabourin-Felix, M., Lindsay, H.,**
761 **Robinson, M. D. and Moss, T.** (2017). A unique enhancer boundary complex on the mouse
762 ribosomal RNA genes persists after loss of Rrn3 or UBF and the inactivation of RNA
763 polymerase I transcription. *PLoS Genet.* **13**, e1006899.
- 764 **Inoue, A. and Aoki, F.** (2010). Role of the nucleoplasmin 2 C-terminal domain in the formation of
765 nucleolus-like bodies in mouse oocytes. *FASEB J. Off. Publ. Fed. Am. Soc. Exp. Biol.* **24**, 485–
766 494.
- 767 **Jachowicz, J. W., Santenard, A., Bender, A., Muller, J. and Torres-Padilla, M.-E.** (2013).
768 Heterochromatin establishment at pericentromeres depends on nuclear position. *Genes Dev.*
769 **27**, 2427–2432.
- 770 **Jansz, N. and Torres-Padilla, M.-E.** (2019). Genome activation and architecture in the early
771 mammalian embryo. *Curr. Opin. Genet. Dev.* **55**, 52–58.
- 772 **Junera, H. R., Masson, C., Geraud, G. and Hernandez-Verdun, D.** (1995). The three-dimensional
773 organization of ribosomal genes and the architecture of the nucleoli vary with G1, S and G2
774 phases. *J. Cell Sci.* **108**, 3427–3441.
- 775 **Kent, T., Lapik, Y. R. and Pestov, D. G.** (2008). The 5' external transcribed spacer in mouse ribosomal
776 RNA contains two cleavage sites. *RNA* **15**, 14–20.
- 777 **Koné, M. C., Fleurot, R., Chebrout, M., Debey, P., Beaujean, N. and Bonnet-Garnier, A.** (2016).
778 Three-Dimensional Distribution of UBF and Nopp140 in Relationship to Ribosomal DNA
779 Transcription During Mouse Preimplantation Development1. *Biol. Reprod.* **94**,
- 780 **Kyogoku, H., Fulka, J., Wakayama, T. and Miyano, T.** (2014). De novo formation of nucleoli in
781 developing mouse embryos originating from enucleolated zygotes. *Development* **141**, 2255–
782 2259.
- 783 **Lavrentyeva, E., Shishova, K., Kagarlitsky, G. and Zatsepina, O.** (2015). Localisation of RNAs and
784 proteins in nucleolar precursor bodies of early mouse embryos. *Reprod. Fertil. Dev.*
- 785 **Le Bouteiller, M., Souilhol, C., Beck-Cormier, S., Stedman, A., Burlen-Defranoux, O., Vandormael-**
786 Pournin, S., Bernex, F., Cumano, A. and Cohen-Tannoudji, M. (2013). Notchless-dependent

- 787 ribosome synthesis is required for the maintenance of adult hematopoietic stem cells. *J. Exp.*
788 *Med.* **210**, 2351–2369.
- 789 **Lehnertz, B., Ueda, Y., Derijck, A. A., Braunschweig, U., Perez-Burgos, L., Kubicek, S., Chen, T., Li, E.,**
790 **Jenuwein, T. and Peters, A. H.** (2003). Suv39h-mediated histone H3 lysine 9 methylation
791 directs DNA methylation to major satellite repeats at pericentric heterochromatin. *Curr. Biol.*
792 **13**, 1192–1200.
- 793 **Maiser, A., Dillinger, S., Längst, G., Schermelleh, L., Leonhardt, H. and Németh, A.** (2020). Super-
794 resolution *in situ* analysis of active ribosomal DNA chromatin organization in the nucleolus.
795 *Sci. Rep.* **10**, 7462.
- 796 **Mangan, H., Gailín, M. Ó. and McStay, B.** (2017). Integrating the genomic architecture of human
797 nucleolar organizer regions with the biophysical properties of nucleoli. *FEBS J.* **284**, 3977–
798 3985.
- 799 **Mars, J.-C., Tremblay, M. G., Valere, M., Sibai, D. S., Sabourin-Felix, M., Lessard, F. and Moss, T.**
800 (2020). The chemotherapeutic agent CX-5461 irreversibly blocks RNA polymerase I initiation
801 and promoter release to cause nucleolar disruption, DNA damage and cell inviability. *NAR*
802 *Cancer* **2**.
- 803 **Mayer, R., Brero, A., von Hase, J., Schroeder, T., Cremer, T. and Dietzel, S.** (2005). Common themes
804 and cell type specific variations of higher order chromatin arrangements in the mouse. *BMC*
805 *Cell Biol.* **6**, 44.
- 806 **Meaburn, K. J.** (2016). Spatial Genome Organization and Its Emerging Role as a Potential Diagnosis
807 Tool. *Front. Genet.* **7**.
- 808 **Miyanari, Y. and Torres-Padilla, M. E.** (2012). Control of ground-state pluripotency by allelic
809 regulation of Nanog. *Nature* **483**, 470–3.
- 810 **Moss, T., Mars, J.-C., Tremblay, M. G. and Sabourin-Felix, M.** (2019). The chromatin landscape of the
811 ribosomal RNA genes in mouse and human. *Chromosome Res.* **27**, 31–40.
- 812 **Mullineux, S.-T. and Lafontaine, D. L. J.** (2012). Mapping the cleavage sites on mammalian pre-
813 rRNAs: Where do we stand? *Biochimie* **94**, 1521–1532.
- 814 **Ogushi, S. and Saitou, M.** (2010). The nucleolus in the mouse oocyte is required for the early step of
815 both female and male pronucleus organization. *J. Reprod. Dev.* **56**, 495–501.
- 816 **Ogushi, S., Palmieri, C., Fulka, H., Saitou, M., Miyano, T. and Fulka, J.** (2008). The Maternal
817 Nucleolus Is Essential for Early Embryonic Development in Mammals. *Science* **319**, 613.
- 818 **Ogushi, S., Yamagata, K., Obuse, C., Furuta, K., Wakayama, T., Matzuk, M. M. and Saitou, M.**
819 (2017). Reconstitution of the oocyte nucleolus in mice through a single nucleolar protein,
820 NPM2. *J. Cell Sci.* **130**, 2416–2429.
- 821 **Padeken, J. and Heun, P.** (2014). Nucleolus and nuclear periphery: Velcro for heterochromatin. *Curr.*
822 *Opin. Cell Biol.* **28**, 54–60.
- 823 **Pederson, T.** (2011). The Nucleolus. *Cold Spring Harb. Perspect. Biol.* **3**, a000638–a000638.

- 824 **Perry, R. P. and Kelley, D. E.** (1970). Inhibition of RNA synthesis by actinomycin D: characteristic
825 dose-response of different RNA species. *J. Cell. Physiol.* **76**, 127–139.
- 826 **Potapova, T. A. and Gerton, J. L.** (2019). Ribosomal DNA and the nucleolus in the context of genome
827 organization. *Chromosome Res.* **27**, 109–127.
- 828 **Probst, A. V., Santos, F., Reik, W., Almouzni, G. and Dean, W.** (2007). Structural differences in
829 centromeric heterochromatin are spatially reconciled on fertilisation in the mouse zygote.
830 *Chromosoma* **116**.
- 831 **Probst, Aline. V., Okamoto, I., Casanova, M., El Marjou, F., Le Baccon, P. and Almouzni, G.** (2010). A
832 Strand-Specific Burst in Transcription of Pericentric Satellites Is Required for Chromocenter
833 Formation and Early Mouse Development. *Dev. Cell* **19**, 625–638.
- 834 **Romanova, L.** (2006). High Resolution Mapping of Ribosomal DNA in Early Mouse Embryos by
835 Fluorescence In Situ Hybridization. *Biol. Reprod.* **74**, 807–815.
- 836 **Sanij, E., Hannan, K. M., Xuan, J., Yan, S., Ahern, J. E., Trigos, A. S., Brajanovski, N., Son, J., Chan, K.**
837 **T., Kondrashova, O., et al.** (2020). CX-5461 activates the DNA damage response and
838 demonstrates therapeutic efficacy in high-grade serous ovarian cancer. *Nat. Commun.* **11**,
839 2641.
- 840 **Savić, N., Bär, D., Leone, S., Frommel, S. C., Weber, F. A., Vollenweider, E., Ferrari, E., Ziegler, U.,**
841 **Kaech, A., Shakhova, O., et al.** (2014). lncRNA Maturation to Initiate Heterochromatin
842 Formation in the Nucleolus Is Required for Exit from Pluripotency in ESCs. *Cell Stem Cell* **15**,
843 720–734.
- 844 **Schindelin, J., Arganda-Carreras, I., Frise, E., Kaynig, V., Longair, M., Pietzsch, T., Preibisch, S.,**
845 **Rueden, C., Saalfeld, S., Schmid, B., et al.** (2012). Fiji: an open-source platform for biological-
846 image analysis. *Nat. Methods* **9**, 676–682.
- 847 **Schindelin, J., Rueden, C. T., Hiner, M. C. and Eliceiri, K. W.** (2015). The ImageJ ecosystem: An open
848 platform for biomedical image analysis. *Mol. Reprod. Dev.* **82**, 518–529.
- 849 **Schneider, C. A., Rasband, W. S. and Eliceiri, K. W.** (2012). NIH Image to ImageJ: 25 years of image
850 analysis. *Nat. Methods* **9**, 671–675.
- 851 **Schöfer, C., Weipoltshammer, K., Almeder, M., Müller, M. and Wachtler, F.** (1996). Redistribution of
852 ribosomal DNA after blocking of transcription induced by actinomycin D. *Chromosome Res.* **4**,
853 384–391.
- 854 **Shishova, K. V. and others** (2011). The fate of the nucleolus during mitosis: comparative analysis of
855 localization of some forms of pre-rRNA by fluorescent in situ hybridization in NIH/3T3 mouse
856 fibroblasts. *Acta Naturae Англоязычная Версия* **3**.
- 857 **Shishova, K. V., Lavrentyeva, E. A., Dobrucki, J. W. and Zatsepina, O. V.** (2015a). Nucleolus-like
858 bodies of fully-grown mouse oocytes contain key nucleolar proteins but are impoverished for
859 rRNA. *Dev. Biol.* **397**, 267–281.
- 860 **Shishova, K. V., Khodarovich, Y. M., Lavrentyeva, E. A. and Zatsepina, O. V.** (2015b). High-resolution
861 microscopy of active ribosomal genes and key members of the rRNA processing machinery
862 inside nucleolus-like bodies of fully-grown mouse oocytes. *Exp. Cell Res.* **337**, 208–218.

- 863 Solovei, I., Kreysing, M., Lanctôt, C., Kösem, S., Peichl, L., Cremer, T., Guck, J. and Joffe, B. (2009).
864 Nuclear Architecture of Rod Photoreceptor Cells Adapts to Vision in Mammalian Evolution.
865 *Cell* **137**, 356–368.
- 866 Stalling, D., Westerhoff, M. and Hege, H.-C. Amira - a Highly Interactive System for Visual Data
867 Analysis. 18.
- 868 Stefanovsky, V. Y., Pelletier, G., Bazett-Jones, D. P., Crane-Robinson, C. and Moss, T. (2001). DNA
869 looping in the RNA polymerase I enhancesome is the result of non-cooperative in-phase
870 bending by two UBF molecules. *Nucleic Acids Res.* **29**, 3241–3247.
- 871 Szabo, Q., Donjon, A., Jerković, I., Papadopoulos, G. L., Cheutin, T., Bonev, B., Nora, E. P., Bruneau,
872 Bantignies, F. and Cavalli, G. (2020). Regulation of single-cell genome organization into
873 TADs and chromatin nanodomains. *Nat. Genet.* **52**, 1151–1157.
- 874 van de Nobelen, S., Rosa-Garrido, M., Leers, J., Heath, H., Soochit, W., Joosen, L., Jonkers, I.,
875 Demmers, J., van der Reijden, M., Torrano, V., et al. (2010). CTCF regulates the local
876 epigenetic state of ribosomal DNA repeats. *Epigenetics Chromatin* **3**, 19.
- 877 van Sluis, M. and McStay, B. (2017). Nucleolar reorganization in response to rDNA damage. *Curr.*
878 *Opin. Cell Biol.* **46**, 81–86.
- 879 van Steensel, B. and Furlong, E. E. M. (2019). The role of transcription in shaping the spatial
880 organization of the genome. *Nat. Rev. Mol. Cell Biol.* **20**, 327–337.
- 881 Wang, Q. T., Piotrowska, K., Ciemerych, M. A., Milenovic, L., Scott, M. P., Davis, R. W. and
882 Zernicka-Goetz, M. (2004). A Genome-Wide Study of Gene Activity Reveals Developmental
883 Signaling Pathways in the Preimplantation Mouse Embryo. *Dev. Cell* **6**, 133–144.
- 884 Zatsepina, O., Baly, C., Chebrout, M. and Debey, P. (2003). The Step-Wise Assembly of a Functional
885 Nucleolus in Preimplantation Mouse Embryos Involves the Cajal (Coiled) Body. *Dev. Biol.* **253**,
886 66–83.
- 887 Zentner, G. E., Balow, S. A. and Scacheri, P. C. (2014). Genomic Characterization of the Mouse
888 Ribosomal DNA Locus. *G3amp58 GenesGenomesGenetics* **4**, 243–254.
- 889
- 890

891 **Figures Legend:**

892

893 **Figure 1: 3D organization of ribosomal sequences (rDNA) is correlated with their**
894 **transcriptional state**

895 (A) 3D organization of rDNA and major satellite sequences at 1-cell and 2-cell stages
896 detected by 3D DNA-FISH using specific probes. Upper panel: single z-section of a
897 representative nucleus of 1-cell (24hphCG), early (E, 36hphCG) and late (L, 48hphCG) 2-cell
898 stages. Lower panel: Amira 3D representation of each nucleus. White (or black, lower panel)
899 arrows indicate clustered rDNA FISH signal juxtaposed to major satellite signal at NPBs
900 surface; green arrows indicated rDNA juxtaposed to round shape major satellite signal and
901 white (or black, lower panel) arrowhead indicate pearl necklace rDNA signal at NPBs
902 surface. (B) Localization of rDNA and major satellite signals in regards to NPBs boundaries
903 at 1-cell and 2-cell stages. Left panel: single z-section of the nucleus with the line
904 corresponding to the Intensity profile measurement in Fiji. Right panel: Fluorescence intensity
905 plot profile along the line across multiple channels (blue dot line for DAPI, the green line for
906 rDNA signal, and red line for major satellite signal). (C) 3D organization of rRNA genes
907 from 4-cell to 8-cell stages detected by 3D DNA-FISH. rDNA FISH signal expands in the
908 inner of the NPBs up to fulfil it completely. Upper panel: z-section of a representative nucleus
909 of early (E) or late (L) 4-cell and 8-cell stage. Lower panel: Amira 3D representation of each
910 nucleus. (D) Localization of rDNA and major satellite signals in regards to NPBs boundaries
911 at 4-cell and 8-cell stages. Left panel: single z-section of the nucleus with the line
912 corresponding to the Intensity profile measurement in Fiji. Right panel: Fluorescence intensity
913 plot profile along the line across multiple channels (blue dot line for DAPI, the green line for
914 rDNA signal, and red line for major satellite signal). DNA is in blue or grey, rDNA in green,
915 and major satellite sequences in magenta. *Scale bar = 5μm*. mPN: maternal Pronucleus; pPN :
916 paternal Pronucleus and NPB: Nucleolar Precursor Body; h phCG : hours post-injection of
917 human Chorionic Gonadotrophin, major: mouse major satellite sequences, rDNA: ribosomal
918 DNA.
919

920 **Figure 2: Features of rDNA spatial organization during pre-implantation development**

921 (A) Spatial organization rDNA surrounding the NPBs. Upper panel: Four kinds of NPBs can
922 be defined depending on their rDNA pattern: Type 1 (T1) displays small dots of rDNA signal,
923 Type 2 (T2) shows spots distributed like a pearl necklace, Type 3 (T3) harbors a thin cloud of
924 rDNA signal and Type 4 (T4) a large cloud of rDNA signal. Stars indicated the NPBs

representative of each type. Scale bar = 5 μ m. **Lower panel:** Quantification of the number of each type of rDNA/NPBs pattern per stage at the 4-cell, 8-cell (early (E) and late (L)) and the early 16-cell stage. Mann-Whitney test was used to compare (two by two) the distribution of the type between stages. **, p-value < 0.01; ***, p-value < 0.001. **(B and C)** Quantification of rDNA total volume (B) and average sphericity (C) per nucleus and stage based on the DNA-FISH signal of the ribosomal sequences. All measurements were done using Imaris 9.6 (Oxford Instruments) from the 2-cell to 16-cell stage. Statistical significance was evaluated using a non-parametric multiple comparison test (nparcomp, R package). ***, p-value < 0.001. The number of nuclei examined per stage is indicated below the stage name.

934

935 **Figure 3: rRNA transcripts organization upon early development**

936 **(A)** rDNA transcripts (green) are visualized by RNA-FISH using a specific probe for the
937 5'ETS region. **Upper panel:** representative nuclei of 2-cell (36h and 45hphCG), 4-cell
938 (60hphCG), 8-cell (72hphCG) and 16-cell (75hphCG) stages embryos. Arrow indicates
939 nascent rRNA labeled with a 5'ETS probe at the surface of an NPB and arrowhead indicates
940 nascent rRNA outside NPB. **Lower panel:** 3D representation of a whole embryo at each stage
941 using Imaris 9.6 for channel segmentation. The hours indicated are “post-injection of hCG”.
942 DNA is labeled in blue and rDNA transcripts in green. *Scale bar = 5 μ m.* **(B)** Schematic
943 representation of the rDNA sequence and position of the rRNA FISH probes used in this
944 study. Each repeat of the mouse ribosomal sequence (X 82564.1) is transcribed in a long
945 mRNA (47S) encoding for 18S, 5.8S, and 28S rRNAs, separated by two external transcribed
946 spacers (5'ETS and 3'ETS) and two internal transcribed spacer (ITS1 and ITS2). **(C)**
947 Quantification of the rRNA transcription at 2-cell (early (E) and late (L)), 4-cell (e and L), 8-
948 cell (E and L), and 16 cell stages by Real-Time qPCR (RT-qPCR) using primers (described in
949 Table S2) specific of 47S long pre-rRNA, of 5'ETS, ITS1 and ITS2 regions. Four to six
950 biological replicates were done by stage, the expression of these pre-RNA was normalized to
951 a fixed amount of luciferase mRNA added before the reverse transcription. Statistical
952 significance was evaluated using a non-parametric multiple comparison test (nparcomp, R
953 package). ***, p-value < 0.001. **(D)** Localization of H3K9ac (green) and nascent rRNA
954 (magenta) by immuno-RNA-FISH from 2-cell to 8-cell stage. Green arrows indicate H3K9ac
955 bright and big foci close or inside the 5'ETS RNA-FISH signal. Pixels (point by white arrows)
956 that correspond to co-localization between H3K9ac and 5'ETS fluorescent channels were
957 identified using Imaris 9.6 software.

958

959 **Figure 4: Inhibition of rRNA transcription by CX-5461 and ActD.**

960 **(A)** Localization using immuno RNA-FISH of nascent rRNA (5'ETS probe in green),
961 Nopp140 (red) and UBF (grey) at 4-cell stage in non treated (Ctrl) and treated embryos (CX-
962 5461 and ActD), nuclei were counterstained with DAPI (blue). Every single z-section of a
963 confocal stack image show representative nuclei. Green arrows point 5'ETS FISH signals, red
964 arrows Nopp140 immunostaining, and grey arrows UBF immunostaining. *Scale bar = 5μm.*
965 **(B and C)** Quantification by RT-qPCR of the relative expression of rRNAs amplified with
966 specific primers for 47S, 5'ETS, ITS1, and ITS2 in control embryos (2-cell, 4-cell and 8 cell
967 stages, green spots) and treated embryos (2-cell and 4-cell stages): with CX-5461 (B, orange
968 spots) and actinomycin D (C, purple spots). Statistical significance between control and
969 treated embryos was evaluated using the Mann-Whitney test (wilcox, R-package). *, p-value
970 < 0.05, **, p-value < 0.01. **(D and E)** Representative confocal images of 4-cell stages nucleus
971 in non-treated (Ctrl) and treated embryos with CX-5461 (D) or Actinomycin D (E). In process
972 pre-rRNAs species were localized by RNA-FISH with specific fluorescent oligoprobes for
973 ITS1 (red) - 18S (green), left panel or ITS2 (red) - 28S (green), right panel. Nuclei were
974 counterstained with DAPI (blue). *Scale bar = 5μm.*

975

976 **Figure 5: Consequences of RNA Pol I Inhibition on the spatial organization of ribosomal
977 sequences**

978 **(A)** 3D organization of rDNA and major satellite sequences at 2-cell stages detected by 3D
979 DNA-FISH using specific probes. Upper panel: single z-section of representative nuclei of
980 non-treated (Ctrl) and treated embryos (CX-5461 and ActD). Lower panel: Amira 3D
981 representation of 2-cell embryos. Green arrows indicate clustered rDNA FISH signal
982 juxtaposed to major satellite signal at NPBs surface **(B)** 3D organization of rDNA and major
983 satellite sequences at 4-cell stages detected by 3D DNA-FISH. Upper panel: single z-section
984 of representative nuclei of non-treated (Ctrl) and treated embryos (CX-5461 and ActD).
985 Lower panel: Amira 3D representation of each embryo. Green arrows indicate clustered
986 rDNA FISH signal and red arrows major satellite sequences FISH signal with a ring/half-ring
987 shape. White arrowhead point major satellite sequences FISH signal with a round shape called
988 chromocenter. **(C and D)** Localization of rDNA and major satellite signals in regards to
989 NPBs boundaries at 2-cell stages (C) and 4-cell stages (D) in non-treated (Ctrl) and treated
990 (CX-5461 or ActD) embryos. Left panel: single z-section of a representative nucleus with the
991 line used to draw with Fiji the Intensity plot profile. Right panel: Fluorescence intensity plot
992 profile along the line across multiple channels (blue dot line for DAPI, the green line for

993 rDNA signal, and red line for major satellite signal). DNA is in blue or grey, rDNA in green,
994 and major satellite sequences in magenta. *Scale bar = 5 μ m*. mPN: major : mouse major
995 satellite sequences, rDNA: ribosomal DNA.
996

997 **Figure 6: Consequences of RNA Pol I Inhibition on rDNA and major satellite sequences**
998 **3D conformation (volume and shape).**

999 **(A and B)** Quantification of rDNA total volume (A) and average sphericity (B) per nucleus
1000 and stage based on the DNA-FISH signal of the ribosomal sequences at 2-cell and 4-cell
1001 stages in non-treated (Ctrl) and treated (CX-5461 or ActD) embryos. The number of nuclei
1002 examined per condition is indicated below the name of the condition (Ctrl in green, CX-5461
1003 in orange, and ActD in purple). **(C and D)** Quantification of major satellite sequence total
1004 volume (C) and average sphericity (D) per nucleus and per stage based on the DNA-FISH
1005 signal, at 2-cell and 4-cell stages in non-treated (Ctrl) and treated (CX-5461 or ActD)
1006 embryos. The number of nuclei examined per condition is indicated below the name of the
1007 condition (Ctrl in pink, CX-5461 in orange, and ActD in purple). All measurements were
1008 done using Imaris 9.6 (Oxford Instruments). Statistical significance was evaluated using a
1009 non-parametric multiple comparison test (nparcomp, R package). ***, p-value < 0.001.
1010

1011 **Figure 7: Consequences of RNA Pol I Inhibition on the expression of major satellite**
1012 **sequences**

1013 **(A and B)** Quantification by RT-qPCR of the relative expression of ncRNA amplified with
1014 specific primers for major satellite sequence in control embryos (2-cell, 4-cell and 8 cell
1015 stages, pink/red spots) and treated embryos (2-cell and 4-cell stages): with CX-5461 (A,
1016 orange spots) and actinomycin D (B, purple spots). Three to four biological replicates were
1017 done by condition, the expression of these ncRNA was normalized to a fixed amount of
1018 luciferase mRNA added before the reverse transcription. Statistical significance between
1019 control and treated embryos was evaluated using the Mann-Whitney test (Wilcox, R-
1020 package). **, p-value < 0.01. **(C)** Major satellite transcripts (magenta) visualized using RNA-
1021 FISH in non treated (Ctrl) in non-treated (Ctrl) and treated (CX-5461 or ActD) embryos from
1022 2-cell (early (E) and late (L)) to 4-cell and 8-cell stages. ncRNAs spots are indicated by red
1023 arrows in treated embryos. **(D)** Localization of nascent rRNAs (green) and major satellite
1024 ncRNAs (red) in mouse embryos from the 4-cell to 16-cell stages by RNA-FISH using
1025 specific probes for 5'ETS region and major satellite sequences. Green arrows indicate a 5'ETS

1026 RNA-FISH signal closed to a major satellite signal (red arrows). Nuclei were counterstained
1027 with DAPI (blue). *Scale bar = 5 μ m.*
1028
1029

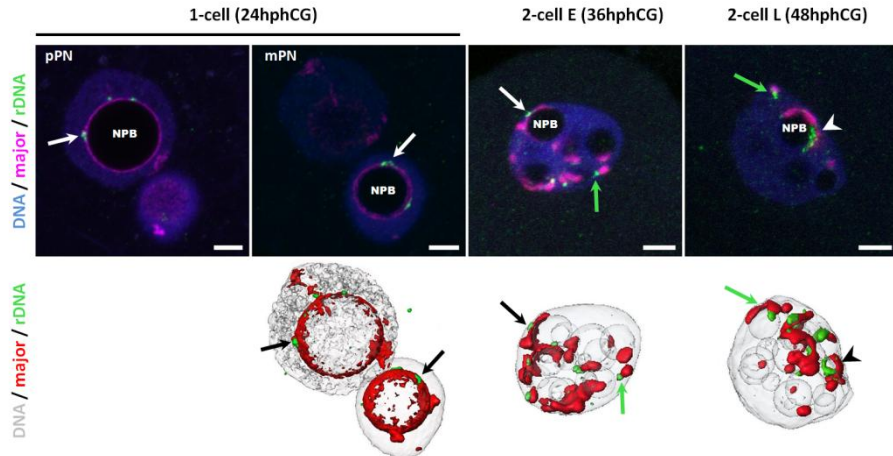
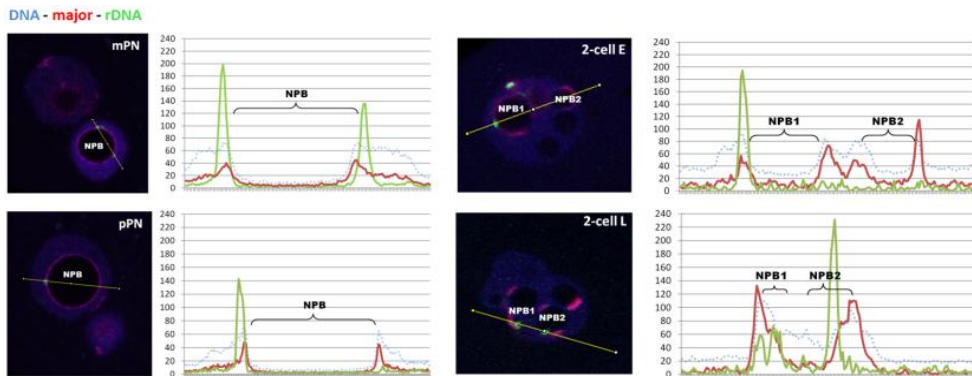
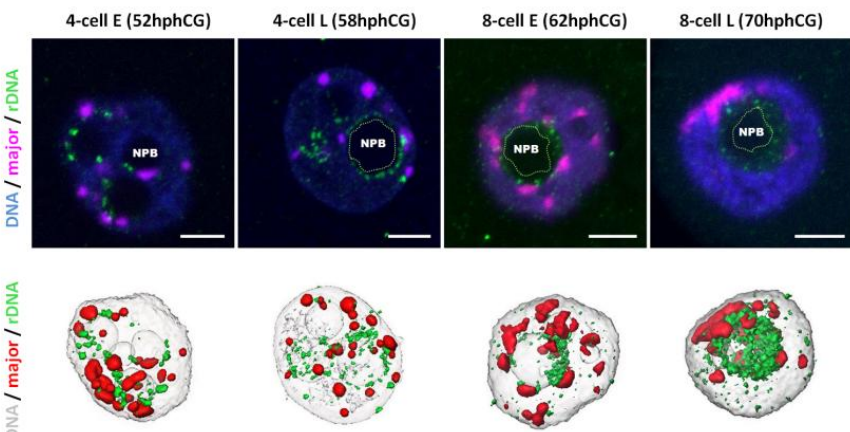
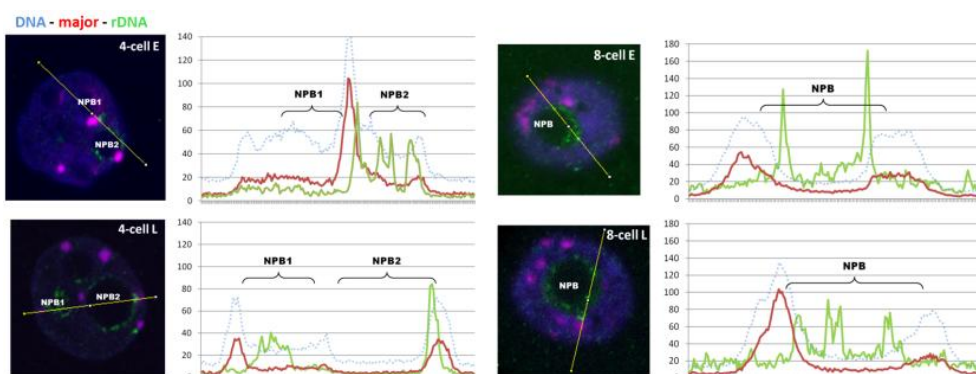
A**B****C****D**

Figure 1 : 3D organization of ribosomal sequences (rDNA) is correlated with their transcriptional state

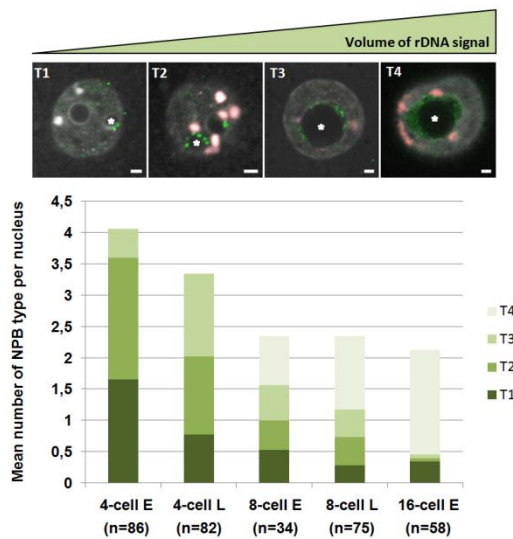
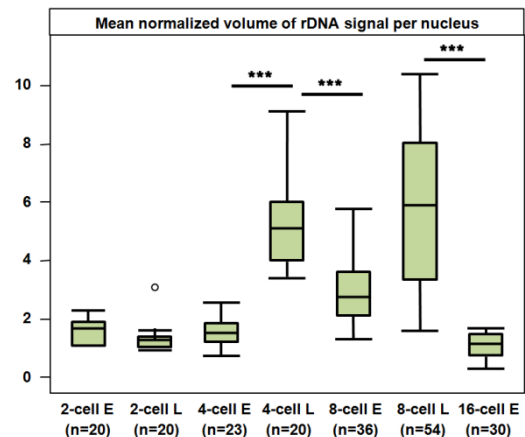
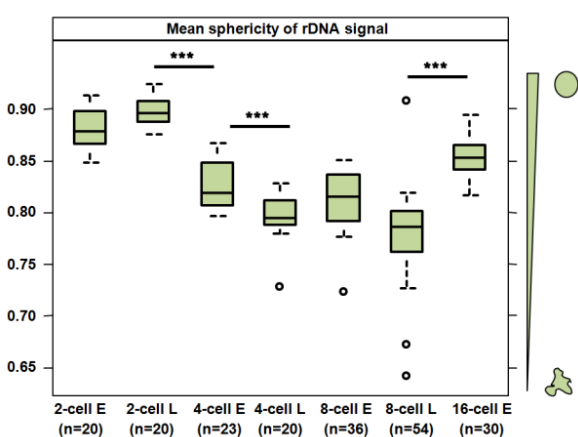
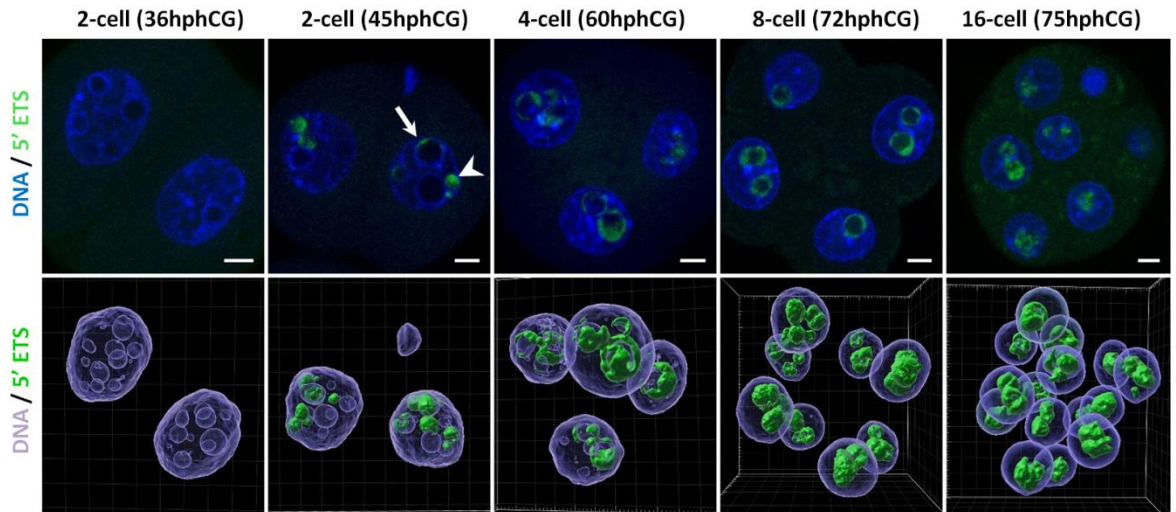
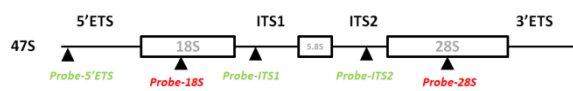
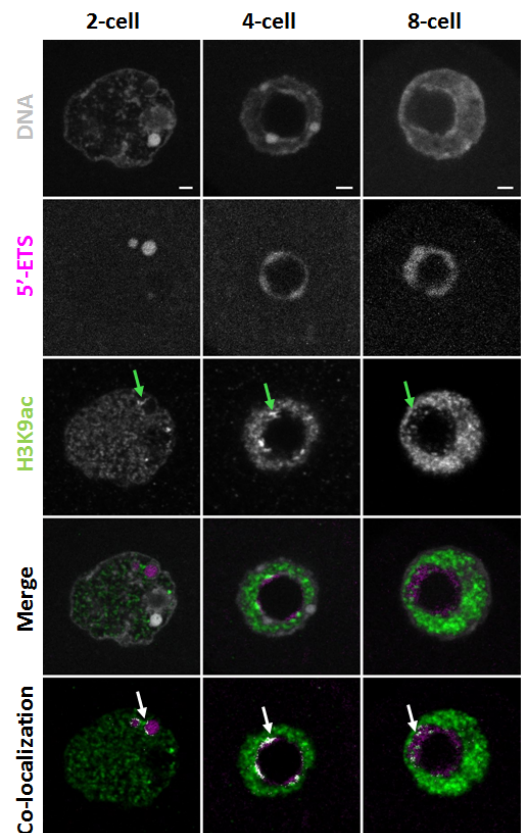
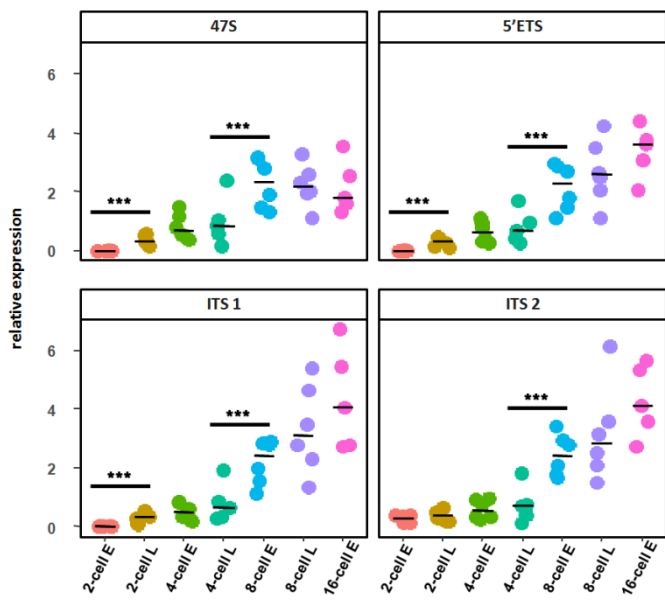
A**B****C**

Figure 2 : Features of rDNA spatial organization during pre-implantation development

A**B****D****C****Figure 3: rRNA transcripts organization upon early development**

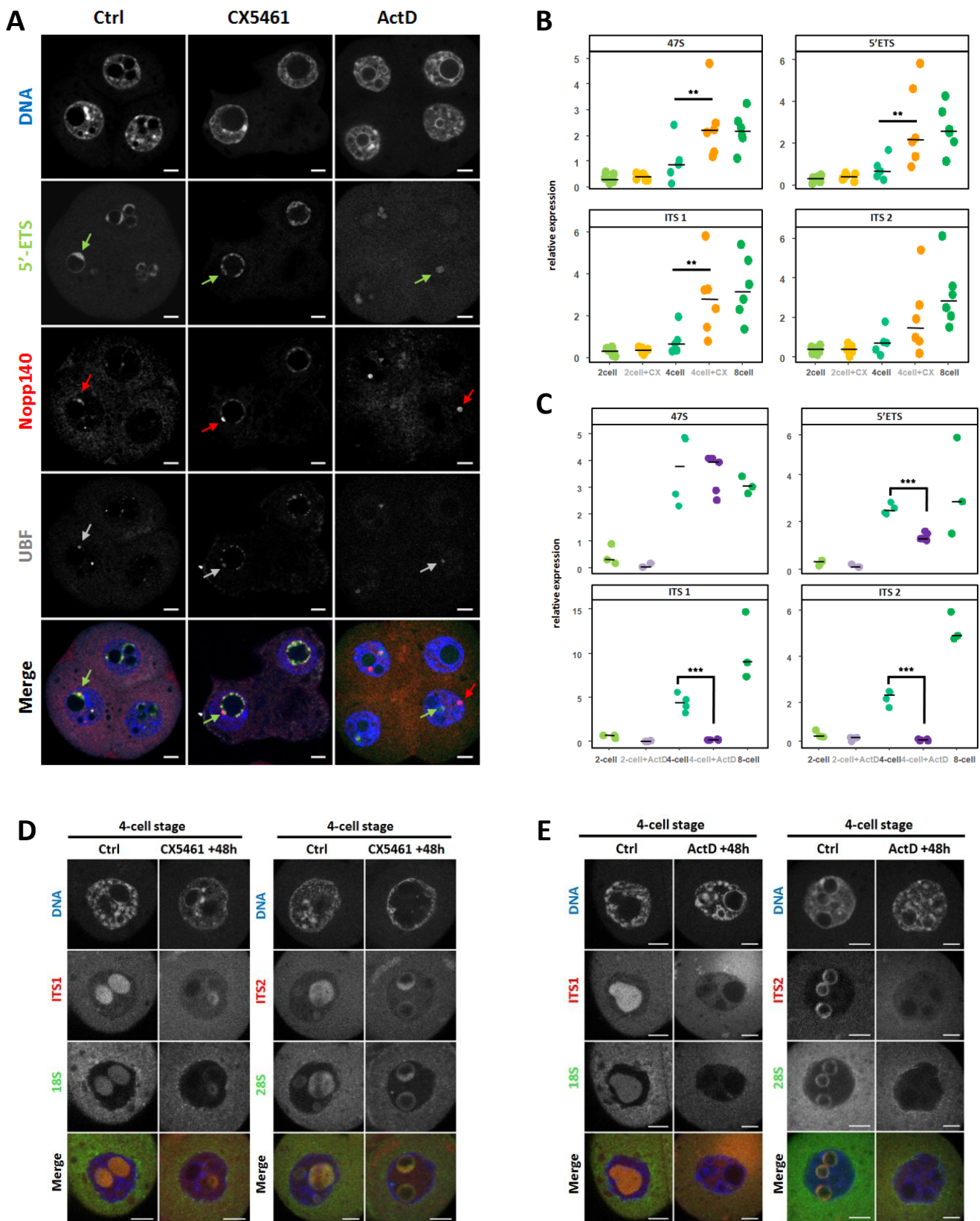


Figure 4: Inhibition of rRNA transcription by CX5461 and ActD

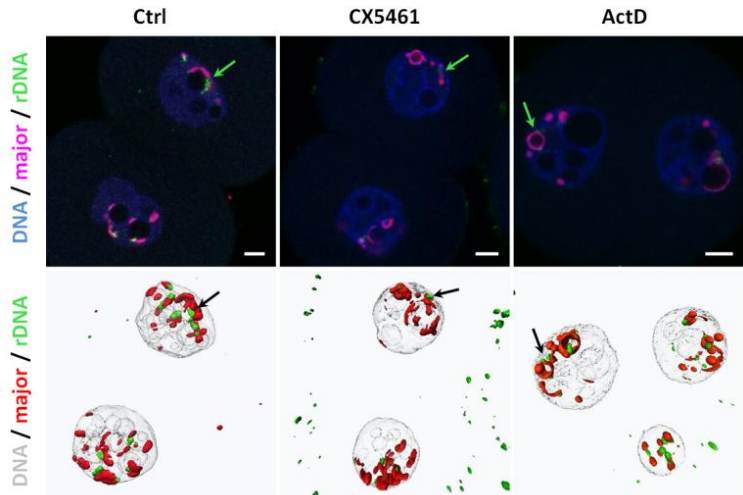
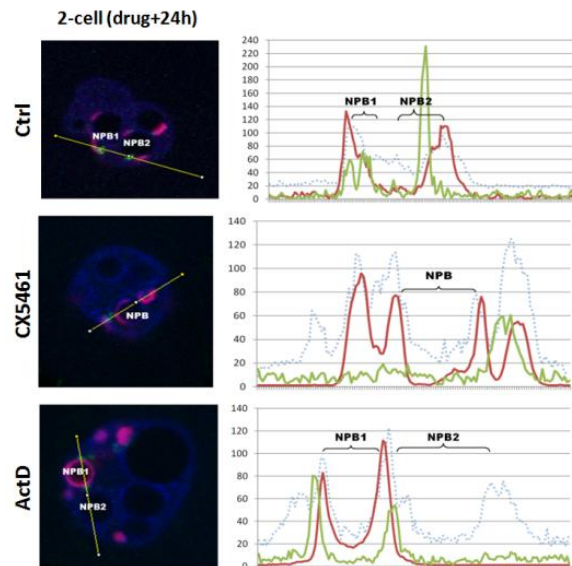
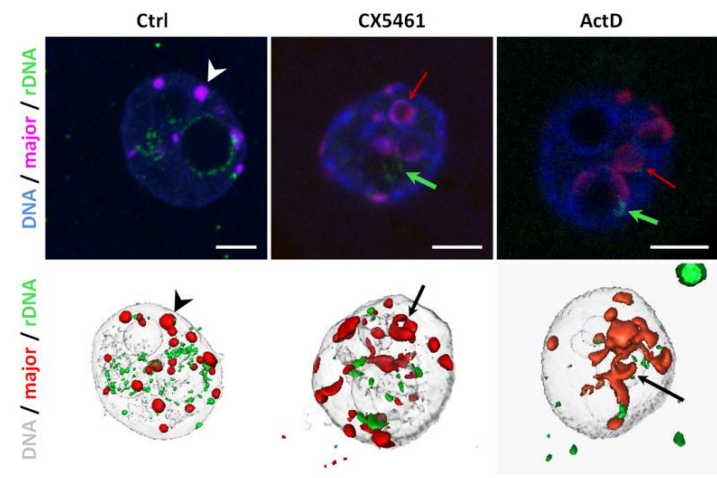
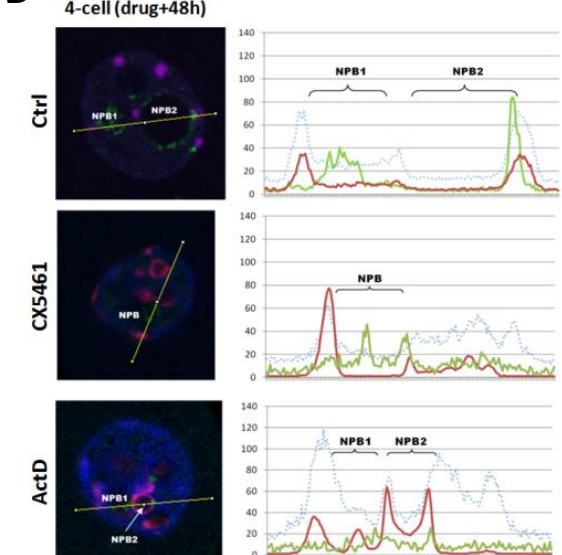
A**C****B****D**

Figure 5: Consequences of RNA Pol I Inhibition on the spatial organization of ribosomal sequences

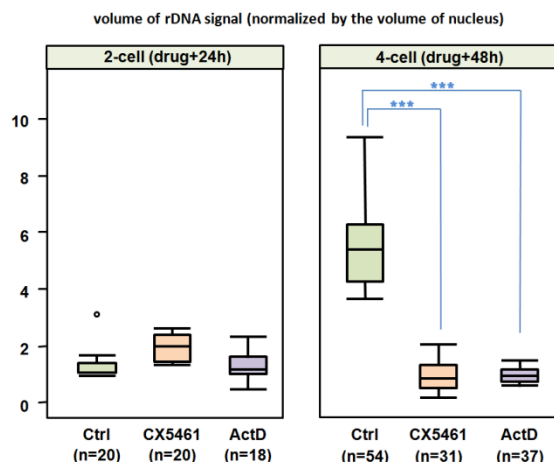
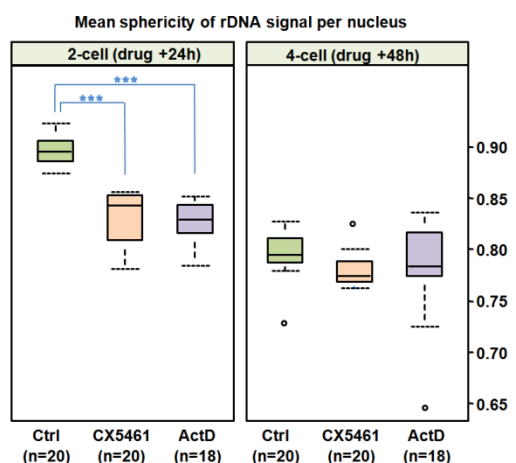
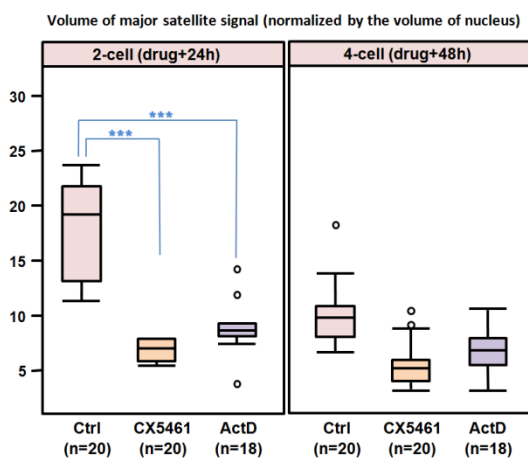
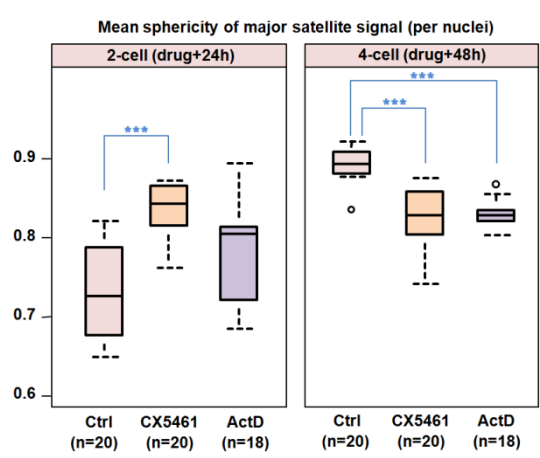
A**B****C****D**

Figure 6: Consequences of RNA Pol I Inhibition on rDNA and major satellite sequences 3D conformation (volume and shape)

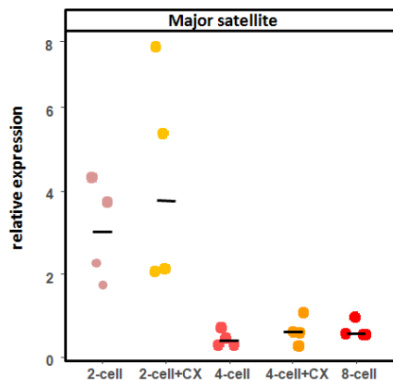
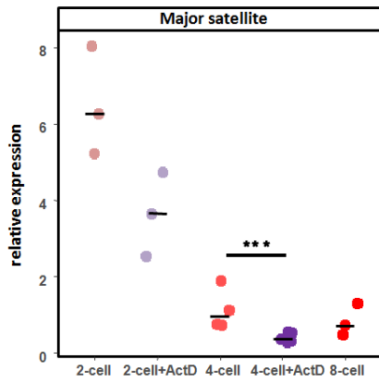
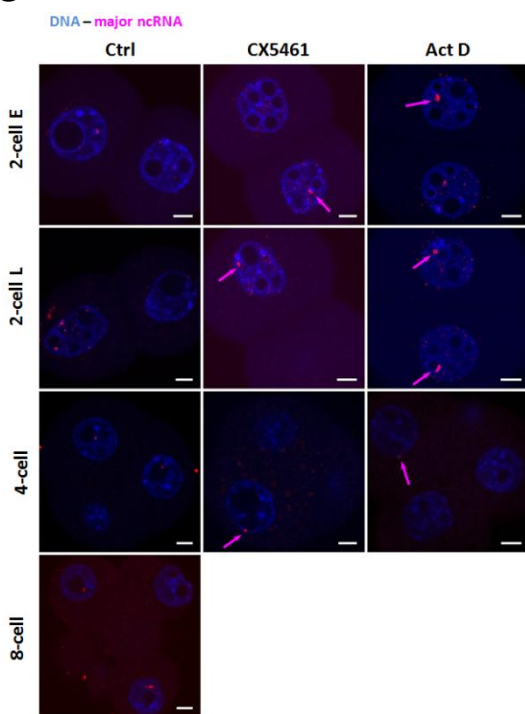
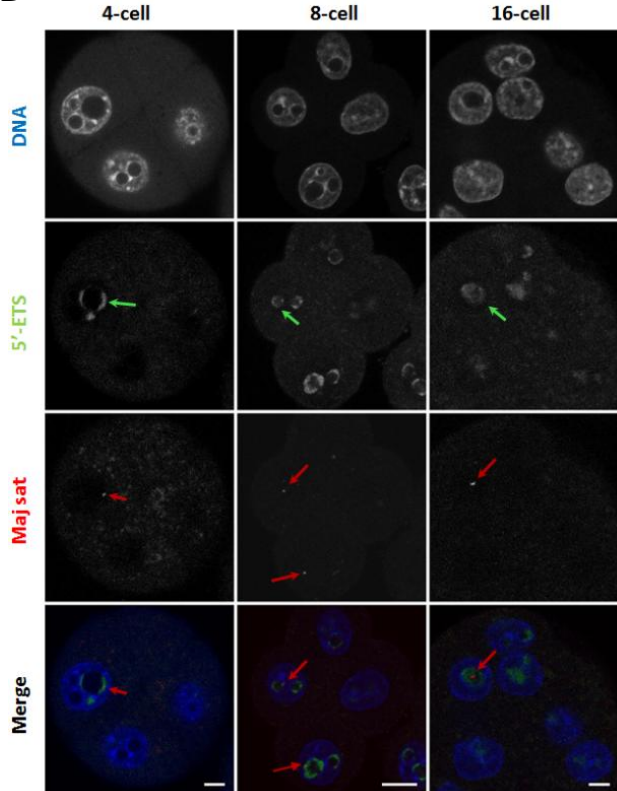
A**B****C****D**

Figure 7 : Consequences of RNA Pol I Inhibition on the expression of major satellite sequences